

INFORMATION TO USERS

This manuscript has been reproduced from the microfilm master. UMI films the text directly from the original or copy submitted. Thus, some thesis and dissertation copies are in typewriter face, while others may be from any type of computer printer.

The quality of this reproduction is dependent upon the quality of the copy submitted. Broken or indistinct print, colored or poor quality illustrations and photographs, print bleedthrough, substandard margins, and improper alignment can adversely affect reproduction.

In the unlikely event that the author did not send UMI a complete manuscript and there are missing pages, these will be noted. Also, if unauthorized copyright material had to be removed, a note will indicate the deletion.

Oversize materials (e.g., maps, drawings, charts) are reproduced by sectioning the original, beginning at the upper left-hand corner and continuing from left to right in equal sections with small overlaps.

Photographs included in the original manuscript have been reproduced xerographically in this copy. Higher quality 6" x 9" black and white photographic prints are available for any photographs or illustrations appearing in this copy for an additional charge. Contact UMI directly to order.

Bell & Howell Information and Learning
300 North Zeeb Road, Ann Arbor, MI 48106-1346 USA

UMI[®]
800-521-0600

THE FLORIDA STATE UNIVERSITY
COLLEGE OF ARTS AND SCIENCES

THE SPRING TRANSITION OF THERMAL STRATIFICATION
ON A MID-LATITUDE CONTINENTAL SHELF

By

STEVEN L. MOREY

A dissertation submitted to the
Department of Oceanography
in partial fulfillment of the
requirements for the degree of
Doctor of Philosophy

Degree Awarded:
Fall Semester, 1999

UMI Number: 9955946

UMI[®]

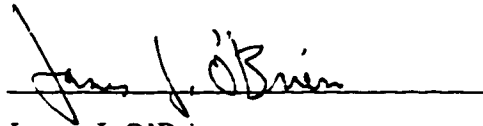
UMI Microform 9955946

Copyright 2000 by Bell & Howell Information and Learning Company.

All rights reserved. This microform edition is protected against
unauthorized copying under Title 17, United States Code.

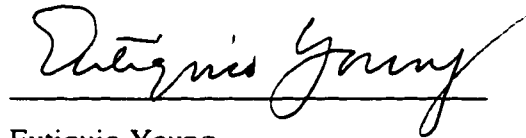
Bell & Howell Information and Learning Company
300 North Zeeb Road
P.O. Box 1346
Ann Arbor, MI 48106-1346

The members of the Committee approve the dissertation of Steven L. Morey
defended on October 4, 1999.



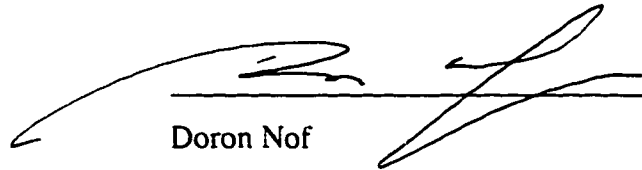
James J. O'Brien

Professor Directing Dissertation




Eutiquio Young

Outside Committee Member



Doron Nof

Committee Member



Allan Clarke

Committee Member



Nancy Marcus

Committee Member

Dedicated to Lloyd and Carol Morey

ACKNOWLEDGEMENTS

I would like to thank Dr. James J. O'Brien, my major professor, who has continued to provide me with the educational opportunities and advice necessary for me to achieve my goals at Florida State University. My sincere appreciation goes to Dr. Paul Martin for the development of, and assistance with, the Sigma Z-level Model. Committee members Dr. Allan Clarke, Dr. Doron Nof, Dr. Nancy Marcus, and Dr. Eutiquio Young have my appreciation for taking time to work with me on this project. I would like to express my gratitude to Dr. Mark Bourassa for his encouragement and scientific input, and COAPS Information Specialist Vince Mariner for assisting me with literature searches. I am grateful as well to countless others at the Center for Ocean – Atmospheric Prediction Studies for their assistance.

Throughout my graduate studies I have received financial support from the Department of Defense through the National Defense Science and Engineering Graduate Fellowship and the University Fellowship from FSU.

TABLE OF CONTENTS

LIST OF TABLES	vi
LIST OF FIGURES	vii
ABSTRACT	x
1. INTRODUCTION	1
2. THE MODEL	9
3. RESULTS	17
3.1 <i>A Simple Model</i>	17
3.2 <i>The Role of Bottom Slope</i>	20
3.3 <i>The Role of Realistic Forcing</i>	25
3.4 <i>Analysis of the T-equation</i>	40
4. DISCUSSION	45
5. SUMMARY	47
REFERENCES	49
BIOGRAPHICAL SKETCH	52

LIST OF TABLES

<u>Table</u>	<u>Page</u>
1. Ocean Model Constants and Parameters	16

LIST OF FIGURES

<u>Figure</u>	<u>Page</u>
1. Schematic of typical winter and summer hydrography in the Middle Atlantic Bight, showing temperature, salinity and density fields	3
2. Typical winter and late spring temperature profiles over the West Florida Shelf	4
3. Temperature-salinity diagram showing typical properties of Middle Atlantic Bight water at the surface on either side of the shelf break front for winter (circles) and summer(squares). Curved lines are density contours in sigma-t units	5
4. Power transfer function of the Asselin Filter for various values of ν where $F^n = Ae^{(i2\pi f\Delta t)}$ and $\overline{F^n} = Be^{(i2\pi f\Delta t)}$	15
5. Temperature profiles and depth averaged temperature representative of wintertime conditions over the West Florida Shelf. The red line shows the depth-averaged temperature resulting from uniform heating of the water column by a spatial uniform heat flux of 40 W/m^2 for 50 days. Note the different cross-shelf scaling	19
6. Initial conditions after spin-up for the sloped shelf (a) vs. flat shelf (b) experiment	22
7. Temperature profiles and depth-averaged temperature for the sloped shelf (a) vs. flat shelf (b) experiment after 60 days of heating	23

<u>Figure</u>	<u>Page</u>
8. Difference in depth-averaged temperature over the continental shelf from 28 km offshore to 178 km offshore. The dashed lines are calculated using the time-integrated form of (24). The solid lines are calculated from the model temperature fields. Results for the sloped bottom are shown in black and the flat bottom results are shown in red	24
9. Vertical grid used in the SZM. 20 evenly spaced sigma coordinates are used above 70 m and 20 evenly spaced z-levels extend below 70 m to 200 m. The free surface is a sigma level. The horizontal grid spacing is 3.5 km. The center of every other vertical grid cell has been plotted	27
10. NCEP Reanalysis daily wind stress and net heat flux from 1974 at 27.6° N, 84.4° W. A 9-day running average has been applied to the smooth overplotted lines. The record has been plotted from Julian day 58 to 150, the duration of the model integration after the winter cooling.....	28
11. Temperature fields and upper 70 m depth-averaged temperatures from (a) Julian day 58, (b) day 69, (c) day 76, (d) day 116, (e) day 132, and (f) day 150. All model fields are spatially smoothed with a 1-2-1 smoother in the horizontal and vertical prior to plotting.....	31
12. Depth-averaged buoyancy frequency squared (N^2) at the 10 m, 20 m, 30 m, and 50 m isobaths on the continental shelf. The fluxes forcing the model are plotted again for reference.....	35
13. Critical Richardson number (R_c) contours (left), temperature fields (center), and temperature profiles from the 20 m isobath (right). Red areas indicate $R_i > R_c$ and blue areas indicate $R_i < R_c$	38
14. Temperature fields (left) and cross-shelf velocity (positive toward shore) (right) during the formation and offshore advection of the cold pool.....	39
15. Term-by-term analysis of the depth-averaged temperature equation integrated in time from Julian day 58 to day 132.....	42

Figure

Page

16. Change in depth-averaged temperature resulting from horizontal and vertical temperature advection since Julian day 58. The greatest temperature change over the integration period occurs during the cold pool formation and offshore advection..... 43

ABSTRACT

The spring transition from the wintertime horizontal thermal stratification to the summertime vertically stratified state on a wide, sloping mid-latitude continental shelf is investigated. The Sigma Z-Level Model (SZM), a new three-dimensional primitive equation numerical ocean model employing a hybrid sigma coordinate and z-level coordinate in the vertical, simulates the continental shelf region. A simple analytical model to describe the heating rate of a well-mixed water column is introduced and applied to the problem to illustrate the importance of bottom slope in determining the evolution of the horizontal thermal stratification. The applicability of this simple model to continental shelf dynamics forced by realistic surface fluxes is verified by running a “pseudo” two-dimensional (x - z) form of the SZM with daily heat and wind stress records from the West Florida shelf. A term-by-term evaluation of the depth-averaged time-integrated temperature equation quantifies the significance of the physical processes that can alter the horizontal temperature gradient. The simple model used to describe the heating rate of a homogeneous water column appears as the dominant balance in the integrated temperature equation, and agrees to the SZM model results from the simulation with realistic forcing to within 31% error over the shelf. Horizontal and vertical advection during periods of downwelling result in faster heating over the inner shelf than predicted by the simple model. It is shown that two processes describe the

spring transition. The first is the erosion of the wintertime horizontal thermal gradient and occurs on a time scale of about two to three months, dependent upon the heat input, when the water column is being heated and mixed periodically. The second process is the formation of the seasonal thermocline following the last strong mixing event. This occurs on a time scale of less than a week under a stabilizing heat flux and light winds completing the spring transition from horizontal to vertical thermal stratification.

1. INTRODUCTION

In temperate latitudes, wide continental shelf waters exhibit seasonal variability of thermal stratification. In the winter, the water is well mixed vertically and is stratified horizontally. The temperature gradient is consistently directed in the offshore direction. That is, the water is colder near the coast and warmer offshore. Horizontal salinity gradients are also directed offshore due to freshwater runoff near the coast. The temperature and salinity gradients have compensatory effects on the horizontal density stratification such that the horizontal density gradient can be directed in either the onshore or offshore direction. In the summer, the horizontal thermal stratification is relaxed and a thermocline develops resulting in vertically stratified water. A consequence of the formation of the seasonal thermocline is a pycnocline due to the dominating effect of the vertical temperature gradient on the density field. The salinity field is in some instances consistent with vertical stratification, but at some locations is characterized by year-round offshore gradients due to the local freshwater input.

The pycnocline formation is important from a dynamical perspective. During the winter when the shelf waters are homogeneous with depth, the oceanic response to low frequency forcing over the shelf is dominated by the barotropic mode. More specifically, the barotropic mode dominates when the condition $N^2 f^2 \alpha^2 \ll 1$ is satisfied, where N is the shelf-average Brunt-Väisälä frequency, f is the Coriolis parameter, and α is the

average shelf bottom slope [*Clarke and Brink*, 1985]. When a pronounced pycnocline develops, the shelf waters behave much like a two-layer system allowing for a first baroclinic mode response [*Millot*, 1990]. Additional impacts of this stabilization of the water column can include the enhancement of primary productivity and the onset of a spring bloom [*Mann and Lazier*, 1991], and the formation of acoustical “shadow zones” [*Caruthers*, 1977].

The Middle Atlantic Bight has a shelf width of about 100 km. The existence of two distinct regimes of stratification, the horizontally stratified wintertime regime and the vertically stratified summertime regime, has been observed on this shelf [e.g., *Bigelow*, 1933; *Bigelow and Sears*, 1935; *Beardsley et al.*, 1985; *Burrage and Garvine*, 1988; *Houghton et al.*, 1988; *Chapman and Gawarkiewicz*, 1993]. The wintertime stratification is horizontal in salinity and temperature with an offshore density gradient, while the summertime stratification is horizontal in salinity and vertical in temperature with a vertical density gradient (Figure 1). That is, the salinity stratification does not show strong seasonal variability and the temperature stratification is largely responsible for the presence of a pycnocline. Hydrographic data from the West Florida shelf suggest similar seasonal stratification states [*Niiler*, 1976; *Clarke*, 1994]. Winter and summer temperature profiles show that the shelf water is strongly destratified in the winter with a horizontal temperature gradient directed in the offshore direction, and strongly stratified vertically in the summer (Figure 2).

Other examples of continental shelves on which similar seasonal variations of stratification have been observed include the Gulf of Lions in the western Mediterranean [*Millot*, 1990], the Sicilian Continental Shelf [*Artale et al.*, 1988], Jervis Bay along the

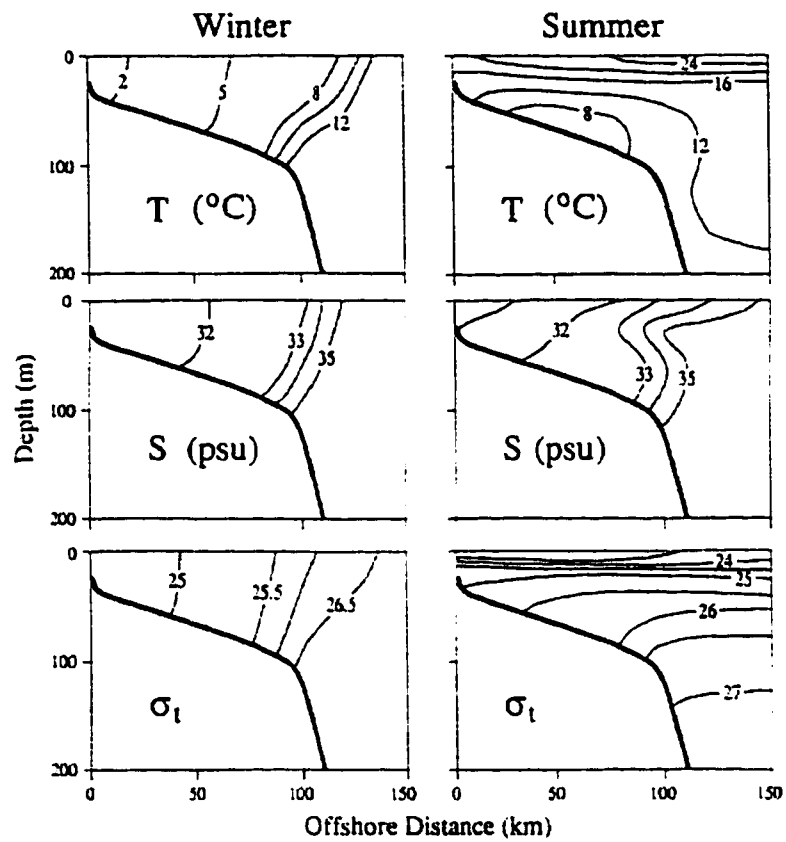


Figure 1. Schematic of typical winter and summer hydrography in the Middle Atlantic Bight, showing temperature, salinity and density fields [*Chapman and Gawarkiewicz, 1993*].

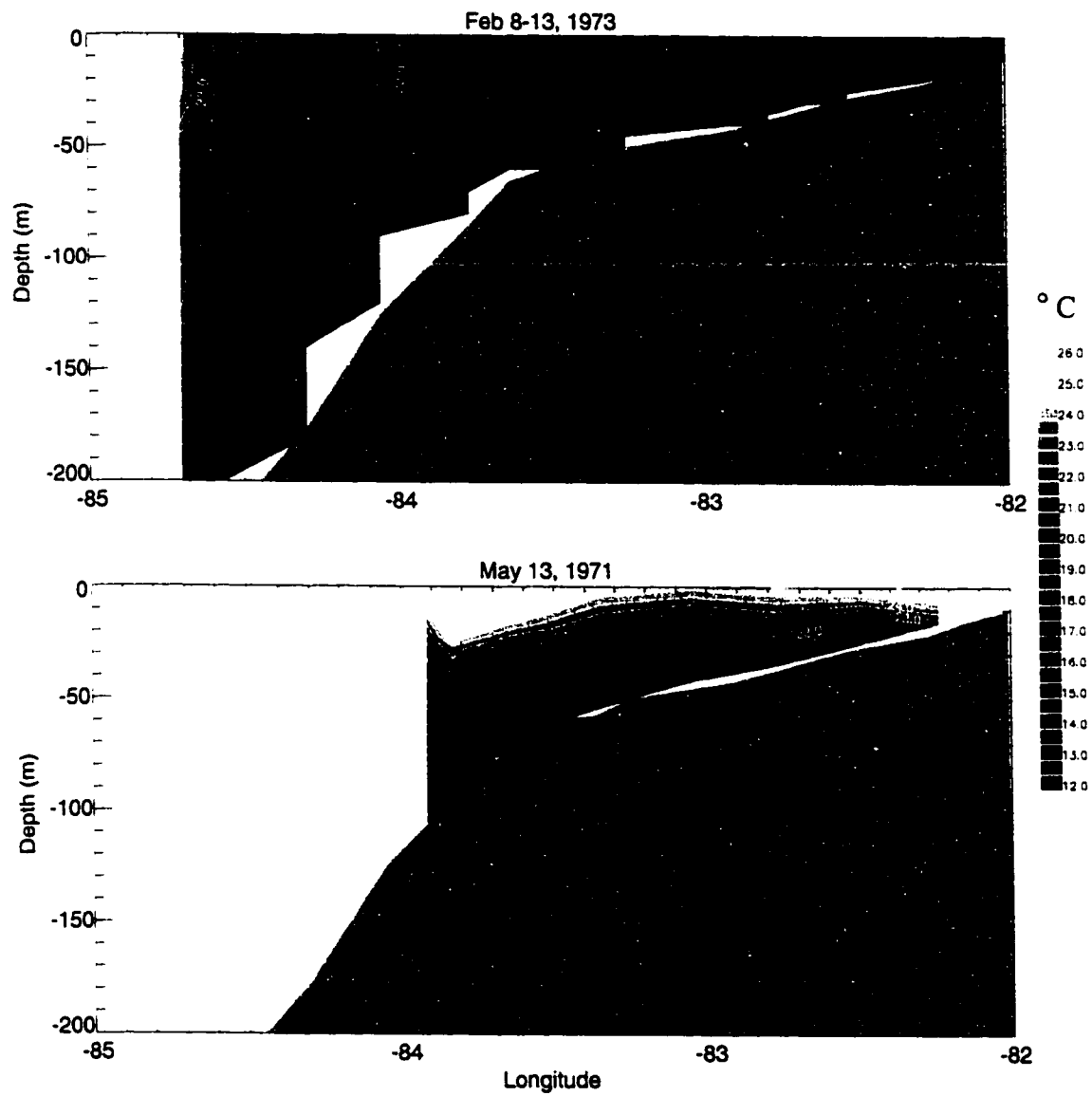


Figure 2. Typical winter and late spring temperature profiles over the West Florida Shelf.

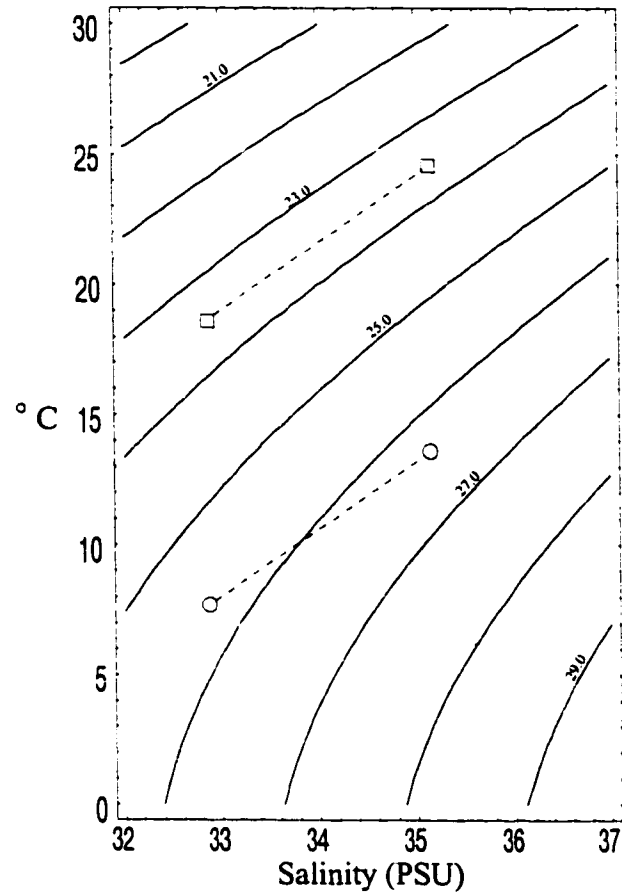


Figure 3. Temperature-salinity diagram showing typical properties of Middle Atlantic Bight water at the surface on either side of the shelf break front for winter (circles) and summer (squares). Curved lines are density contours in sigma-t units. (After *Chapman and Gawarkiewicz [1993]*).

eastern Australian coast [*Symonds and Gardiner-Garden*, 1994], and the South Brazil Bight [*Stech and Lorenzzetti*, 1992]. As a counterexample, the Oregon continental shelf exhibits a spring transition from a vertically stratified winter regime to a horizontally stratified summer regime. This is because the stratification on this very narrow shelf (the 200 m isobath is found only about 25 km offshore) is largely a result of summertime coastal upwelling and wintertime coastal downwelling [*Gilbert et al.*, 1976].

Chapman and Gawarkiewicz [1993] demonstrated that the change from horizontal density stratification in the winter to the summertime vertical stratification could be a result only of uniform surface heating. If a uniform surface density flux resulting from solar heating were applied to a horizontally stratified ocean, then the horizontal density gradients would remain. The authors proposed, however, that a surface heat flux could reduce the horizontal density gradients across the shelf-break front if the nonlinearity of the equation of state was considered (Figure 3). A one-dimensional diffusion model initialized with temperature and salinity fields containing only horizontal gradients was forced with a uniform constant heating at the surface. The model was run with constant and depth-dependent vertical mixing and no other processes were allowed for in the model. After 180 days, vertical density gradients were evident, and the remaining horizontal density gradients were much weaker when density was calculated from a nonlinear equation of state over a linear equation of state.

The classic argument to describe the spring transition from the wintertime horizontal stratification to the summertime vertical stratification has been that the relaxation of the winds during the spring combined with the increased solar heating allows a thermocline, and thus a pycnocline, to form. Though the formation of a seasonal

thermocline is a fairly well understood process, it is not obvious that this can reduce a horizontal temperature gradient. *Chapman and Gawarkiewicz* [1993] have reasoned that the nonlinearity of the equation of state can account for the elimination of horizontal stratification by spatially uniform heating, but their argument is only valid for certain salinity and temperature ranges. Consider the higher wintertime temperatures that exist over the West Florida Shelf water, for example. Typical winter water temperatures range from 18°C onshore to over 22°C offshore (Figure 2). The simple demonstration for the Middle Atlantic Bight (Figure 3) no longer works because for reasonable salinity values, the equation of state becomes nearly linear at these higher temperatures (the density contours become nearly parallel on the T-S diagram). The angle between the σ_t contours and a line connecting the onshore and offshore water parcel properties will not change substantially if only the temperature is uniformly raised, indicating that there would be no change in the horizontal density gradient. Thus, some other process or processes are responsible for altering the density gradients.

The salinity characteristics of continental shelves are largely a product of local freshwater runoff and can vary wildly from shelf to shelf, and even from year to year, but the distinct winter and summer regimes of temperature stratification are a defining feature of wide mid-latitude continental shelf dynamics. Additionally, the summertime vertical thermal stratification has a dominating effect on the density field. The formation of the wintertime horizontal temperature gradient by convective cooling has been examined in detail [*Symonds and Gardiner-Garden*, 1994; *Pringle* 1998], but how this gradient is eroded and reversed is not yet fully understood. The purpose of this investigation is

therefore to determine the processes responsible for the spring transition of the thermal stratification on a mid-latitude continental shelf.

The paucity of observations with adequate spatial resolution and temporal sampling concurrent with the spring transition in temperature stratification on a wide mid-latitude continental shelf makes this an ideal subject for a numerical modeling study. The problem will be investigated using a recently developed model with a hybrid sigma and z-level vertical coordinate. The importance of surface momentum and heat fluxes and shelf topography on the temperature stratification is examined. It is found that a sloping bottom is crucial to the erosion of the horizontal temperature gradient. A simple model for the temperature change of a well-mixed water column subject to a surface heat flux is introduced. This model is applied to the problem of relaxing a horizontal temperature gradient by application of a spatially uniform heat flux. A term-by-term analysis of the depth-averaged time-integrated temperature equation demonstrates the applicability of this simple model to a realistic ocean, but shows that horizontal and vertical advection of temperature can significantly alter the horizontal temperature gradient during a downwelling event.

2. THE MODEL

The spring transition of thermal stratification will be investigated using the Sigma Z-Level Model (SZM) [*Martin*, 1998] to simulate the continental shelf dynamics. The modeled region will consist of a continental shelf with a shelf break leading to an open boundary toward the deep ocean. Sigma coordinates (SC), or terrain following coordinates, are often employed in ocean models over coastal and shelf regions. SC are defined such that a σ surface is everywhere a constant fraction of the total water depth. That is,

$$\sigma = \frac{z - \zeta}{\zeta + H} \quad (1)$$

where $z = 0$ at the resting surface and is positive upward, ζ is the elevation of the free surface, and H is the undisturbed depth of the water column. Thus, σ varies from 0 at the free surface to -1 at the bottom. The use of a SC system is ideal over the shelf because it provides for increased vertical resolution in shallow water and prevents the need for exactly matching the model topography to fixed-depth grid cells. Near steep topography such as the shelf break, however, computing the horizontal pressure gradients in SC can produce large errors. The pressure gradient in SC is the sum of two terms. In the x -direction (neglecting deviations in the free surface),

$$\left. \frac{\partial p}{\partial x} \right|_z = \left. \frac{\partial p}{\partial x} \right|_\sigma - \frac{\sigma}{H} \frac{\partial p}{\partial \sigma} \frac{\partial H}{\partial x}. \quad (2)$$

The first term on the RHS involves the gradient of pressure along a constant sigma surface and the second involves the gradient of the bottom topography. Near steep topography these two terms will be large, comparable in magnitude, and opposite in sign. Thus, a small error in computing either term can result in a large error in computing the pressure gradient term [Haney, 1991].

The horizontal pressure gradient can be accurately computed by using z-level, or fixed-depth, coordinates (ZC). ZC cannot, however, provide for increased vertical resolution in shallow water. In addition, implementing a free surface requires special treatment of the surface layer. *Martin* [1998] combined ZC and SC in the SZM developed at the Naval Research Laboratory. SC are used down to a given depth, and ZC extend below this fixed depth to the bottom. This hybrid vertical coordinate system allows for more accurate computation of the pressure gradient near a sharply sloping bottom, as well as for the benefits of SC on the shelf.

The SZM uses the hydrostatic, Boussinesq, and incompressible approximations, and allows for a free surface. The model equations are

$$\frac{\partial u}{\partial t} = -\nabla \cdot (\mathbf{v}u) + fv - \frac{1}{\rho_0} \frac{\partial p}{\partial x} + \nabla_h (A_M \nabla_h u) + \frac{\partial}{\partial z} (K_M \frac{\partial u}{\partial z}) \quad (3)$$

$$\frac{\partial v}{\partial t} = -\nabla \cdot (\mathbf{v}v) - fu - \frac{1}{\rho_0} \frac{\partial p}{\partial y} + \nabla_h (A_M \nabla_h v) + \frac{\partial}{\partial z} (K_M \frac{\partial v}{\partial z}) \quad (4)$$

$$\frac{\partial p}{\partial z} = -\rho g \quad (5)$$

$$\nabla \cdot \mathbf{v} = \frac{\partial u}{\partial x} + \frac{\partial v}{\partial y} + \frac{\partial w}{\partial z} = 0 \quad (6)$$

$$\frac{\partial \zeta}{\partial t} = -\frac{\partial((\zeta + H)\bar{u})}{\partial x} - \frac{\partial((\zeta + H)\bar{v})}{\partial y} \quad (7)$$

$$\frac{\partial T}{\partial t} = -\nabla \cdot (\mathbf{v}T) + \nabla_h (A_H \nabla_h T) + \frac{\partial}{\partial z} (K_H \frac{\partial T}{\partial z}) \quad (8)$$

$$\frac{\partial S}{\partial t} = -\nabla \cdot (\mathbf{v}S) + \nabla_h (A_H \nabla_h S) + \frac{\partial}{\partial z} (K_H \frac{\partial S}{\partial z}) \quad (9)$$

$$\rho = \rho(T, S, z). \quad (10)$$

The boundary conditions at the surface are

$$\rho_0 K_M \frac{\partial u}{\partial z} = \tau^x \quad (11)$$

$$\rho_0 K_M \frac{\partial v}{\partial z} = \tau^y \quad (12)$$

$$\rho_0 K_H \frac{\partial T}{\partial z} = \frac{Q_b + Q_e + Q_s}{c_p} = \frac{Q}{c_p} \quad (13)$$

$$K_H \frac{\partial S}{\partial z} = S|_{z=0} (E_v - P_r) \quad (14)$$

and at the bottom,

$$K_M \frac{\partial u}{\partial z} = -c_b u |\mathbf{v}| \quad (15)$$

$$K_M \frac{\partial v}{\partial z} = -c_b v |\mathbf{v}| \quad (16)$$

$$K_H \frac{\partial T}{\partial z} = 0 \quad (17)$$

$$K_H \frac{\partial S}{\partial z} = 0. \quad (18)$$

In these equations, T is the potential temperature (henceforth referred to simply as temperature), S is the salinity, A_M and A_H are the horizontal eddy coefficients for momentum and for scalar fields, respectively, K_M and K_H are vertical eddy coefficients for momentum and scalar fields, barred variables are the depth-averaged variables, ζ is the elevation of the free surface above the undisturbed value at $z = 0$, and H is the bottom depth. In the surface boundary conditions, τ^x and τ^y are the x and y components of the surface wind stress, Q_b , Q_e , and Q_s are the net long wave and latent and sensible surface heat fluxes, and Q is the net surface heat flux. E_v and P_r are the surface evaporation and precipitation rates, and c_p is the specific heat of seawater. The bottom stress is parameterized by a quadratic drag law with drag coefficient c_b that is calculated by

$$c_b = \max \left[\frac{\kappa^2}{\log^2 \left(\frac{\Delta z_b}{2z_0} \right)}, c_{b_{\min}} \right]. \quad (19)$$

Δz_b is the bottom layer thickness, z_0 is the bottom roughness, $\kappa = 0.4$ is von Karman's constant, and $c_{b_{\min}}$ is a minimum value for c_b .

The vertical eddy coefficients are calculated from the Mellor-Yamada Level 2 (MYL2) turbulence closure scheme [Mellor and Yamada, 1982], which has been shown to give turbulence mixing scales and turbulent layer depths comparable to the more computationally demanding Mellor-Yamada Level 2.5 turbulence closure scheme [Martin *et al.*, 1998]. Horizontal eddy mixing coefficients are specified as the maximum

of a background value A_0 and the value needed to keep the grid-cell Reynolds number below a maximum specified value R_{e_h} . For example, in the x-direction,

$$A_H = \max(A_{H_0}, \frac{u\Delta x}{R_{e_h}}) \quad (20)$$

$$A_M = \max(A_{M_0}, \frac{u\Delta x}{R_{e_h}}). \quad (21)$$

A similar form of the model equations in SC can be found in *Blumberg and Mellor* [1987]. Using the hybrid vertical coordinate, the transformation from ZC to SC is given by

$$\sigma = \frac{z - \zeta}{\zeta + \min(H, z_s)} \quad (22)$$

where z_s is the specified depth below which ZC are used. Thus, σ varies from 0 at the free surface to -1 at the bottom interface of the lowest sigma layer. Each sigma layer is a fixed fraction of the total depth of the sigma layers.

The SZM uses a staggered Arakawa C grid. Spatial interpolations are second-order centered averages and spatial gradients use second-order centered differences. The model employs a standard leapfrog time-stepping scheme in which the advection, baroclinic pressure gradient, and Coriolis terms are centered in time at the current time step n . Horizontal diffusion terms are computed at $n-1$, and vertical mixing terms are treated implicitly. An Asselin filter given by

$$\overline{F^n} = F^n + \nu (\overline{F^{n-1}} - 2F^n + F^{n+1}) \quad (23)$$

is applied to the model fields at the end of each time step, where ν has a typical value of 0.05. Here, the overbar denotes the filtered value of the variable. This type of filter

damps out the computational mode when using leapfrog time differencing [Asselin, 1972] (Figure 4). The free-surface mode is calculated implicitly, such that the surface pressure gradient and divergence terms in the surface elevation equation have a component at the time level $n+1$.

For the experiments used in this investigation, the SZM is run in a “pseudo” two-dimensional mode by employing a total of four grid points (two interior grid points) and periodic boundary conditions in the along-shore direction. This allows the use of a three-dimensional model for a two-dimensional problem without actually converting the model to two-dimensional form. The domain extends from the coast across the shelf and shelf-break to an open boundary at the deep ocean. All scalar fields at the open boundaries are relaxed to specified values for inflow and Orlanski radiation [Orlanski, 1976] is used for outflow. SC are used to the depth of the shelf break, and ZC are used below as is described in the next section. The constants and model parameters used in this study are shown in Table 1.

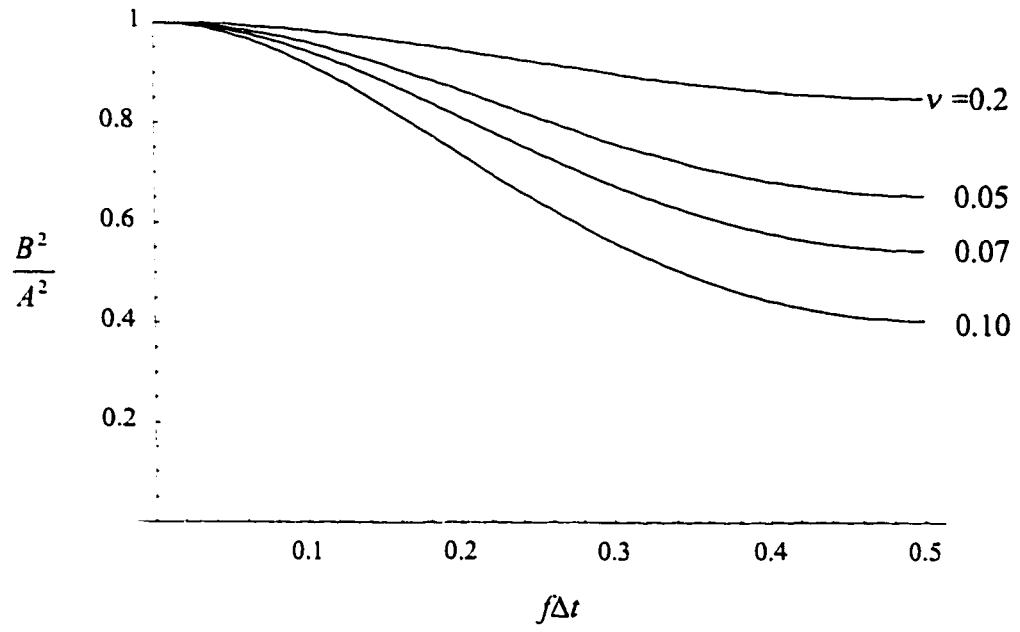


Figure 4. Power transfer function of the Asselin Filter (23) for various values of ν where $F^n = Ae^{(i2\pi f\Delta t)}$ and $\bar{F}^n = Be^{(i2\pi f\Delta t)}$.

Table 1. Ocean model constants and parameters.

Symbol	Description	Value
Δx	Horizontal grid spacing	3.5 km
Δt	Time step	900 s
f	Coriolis parameter	$1.0147 \times 10^{-5} \text{ s}^{-1}$
A_{M_0}	Minimum horizontal eddy coefficient for momentum	$20 \text{ m}^2/\text{s}$
A_{H_0}	Minimum horizontal eddy coefficient for scalars	$20 \text{ m}^2/\text{s}$
R_{e_k}	Maximum grid-cell Reynolds number	100
K_{M_0}	Minimum vertical eddy coefficient for momentum	$1.0 \text{ cm}^2/\text{s}$
K_{H_0}	Minimum vertical eddy coefficient for scalars	$0.1 \text{ cm}^2/\text{s}$
z_0	Bottom roughness	0.3 cm
$c_{b_{\min}}$	Minimum bottom drag coefficient	0.0025
ν	Parameter for Asselin filter	0.05

3. RESULTS

3.1 A simple model

Consider a water column subject to a (positive downward) net surface heat flux $Q(t)$ (W/m^2) and insulated at the bottom. There is no horizontal mixing or horizontal advection. The mean temperature T of a water column of height H will change at the rate

$$\frac{dT}{dt} = \frac{Q(t)}{\rho_0 c_p H} . \quad (24)$$

Here, c_p is the specific heat of the water and ρ_0 is the average density. Since the time rate of change of temperature is inversely proportional to the water column depth, a shallower water column will heat more rapidly than a deeper water column subject to the same positive surface heat flux.

Noh and Fernando [1995] demonstrated by way of a laboratory experiment that a fluid column subject to a stabilizing surface buoyancy flux, but mixed vigorously enough to prevent vertical stratification, had a decrease in density with time which was uniform with depth. Thus, if the buoyancy flux takes the form of a heat flux, a well-mixed water column will be heated uniformly. Under the assumptions made in the formulation of (24), a vertically mixed body of water over a sloping bottom subject to a spatially uniform heat flux will, at all depths, have a temperature gradient tendency positive in the direction of the shallower water.

As an example, consider a vertically mixed body of water over a sloping bottom of depth $H(x) = mx$. Then the change in temperature from some time interval t_0 to t will be (neglecting free surface variations)

$$\Delta T = \frac{\int_{t_0}^t Q(t) dt}{\rho_0 c_p m x}. \quad (25)$$

That is, ΔT will increase hyperbolically toward the coast. Obviously, this becomes unphysically large in extremely shallow water. Nevertheless, the process described by (24) and (25) has been shown to reasonably describe the change in water temperature due to wintertime cooling over mid-latitude continental shelves [Symonds and Gardiner-Garden, 1994; Pringle, 1998].

An example representative of the West Florida shelf demonstrates how a spatially uniform constant heat flux could result in the relaxation of a wintertime horizontal temperature gradient. The cross-shelf temperature difference over the West Florida shelf near the Southwest Florida coast in the Gulf of Mexico could be reduced from 3° C to nearly 0° C by calculating ΔT from (24) applying a constant heat flux of 40 W/m² for 50 days (Figure 5). This example is clearly too simplistic to represent all the processes that may be responsible for altering the shelf water stratification, yet it demonstrates that the simplest thermodynamic forcing and ocean physics could account for the relaxation of the offshore temperature gradient. The question remains whether or not (24) can adequately describe the erosion of the offshore temperature gradient without the assumptions made in developing this simple model. The roles of horizontal advection

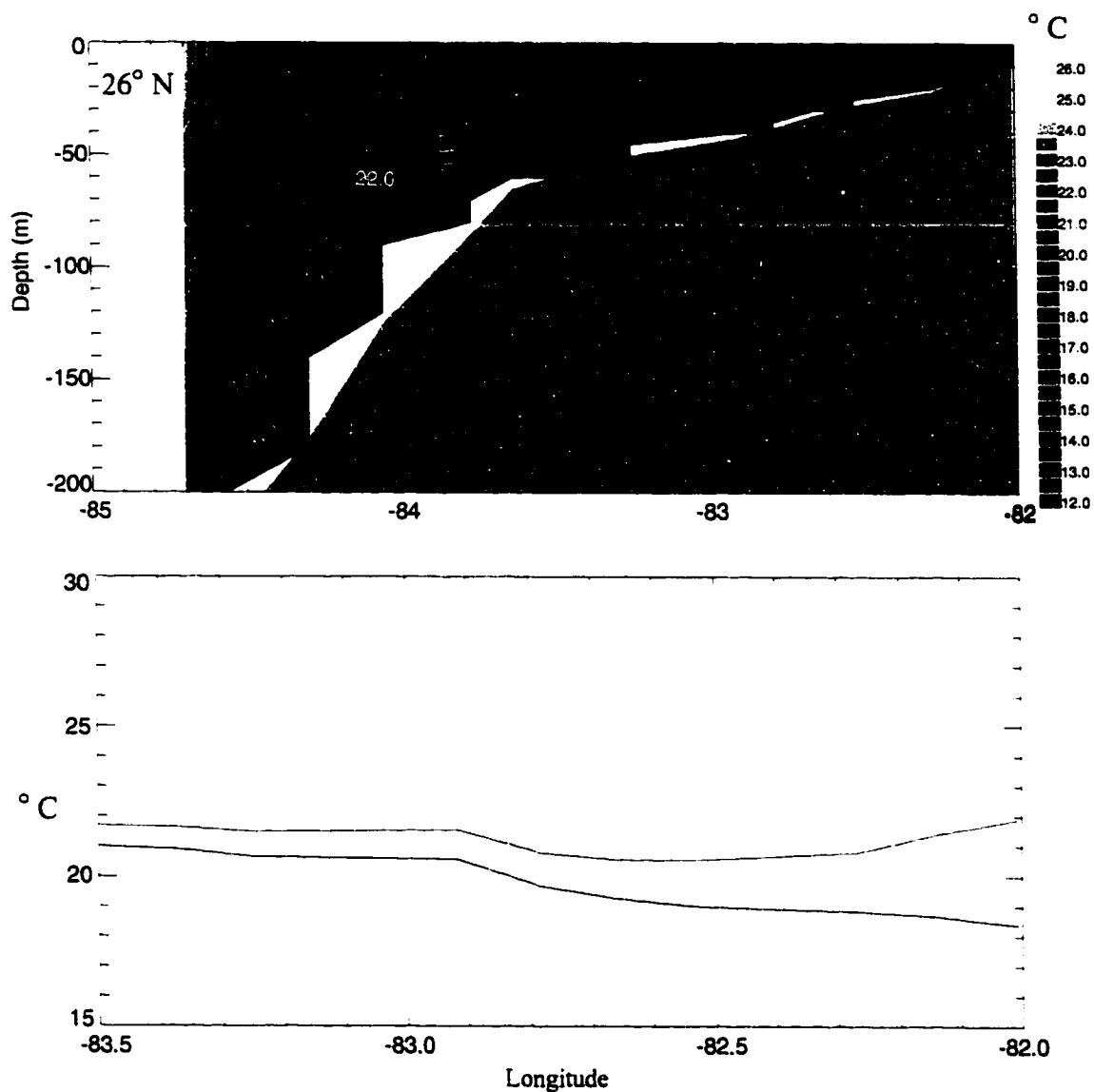


Figure 5. Temperature profiles and depth-averaged temperature representative of wintertime conditions over the West Florida Shelf. The red line shows the depth-averaged temperature resulting from uniform heating of the water column by a spatially uniform heat flux of 40 W/m^2 for 50 days. Note the different cross-shelf scaling.

and mixing must be considered in the presence of realistic forcing and dynamics of continental shelf waters.

3.2 *The role of bottom slope*

In the model described by (24), a spatially uniform surface heat flux applied to a body of water with constant H cannot alter a horizontal temperature gradient. A sloping bottom is necessary for the relaxation or reversal of a temperature gradient directed toward deeper water. The effect of the bottom slope on an existing horizontal temperature gradient is further investigated here using the SZM with idealized forcing and topography.

The model domains are chosen to represent a sloping continental shelf and a flat continental shelf. The topography for the sloped bottom experiment is defined by a 7 m depth at the first ocean grid point next to the coast and a bottom slope of

$$m = \begin{cases} 1.04762 \times 10^{-4}, & x < 21 \text{ km} \\ 3.36562 \times 10^{-4}, & 21 \text{ km} < x < 203 \text{ km} \\ 18.5000 \times 10^{-4}, & 203 \text{ km} < x < 273 \text{ km} \\ 0, & 273 \text{ km} < x \end{cases} \quad (26)$$

where x is the distance from the coast. For $x > 273$ km, the bottom is 200 m deep to the open boundary 413 km offshore. The flat shelf model domain consists of a shelf of constant depth 25.2 m extending to the shelf break 178.5 km from the coast. At the shelf break, the seafloor slopes downward to a depth of 200 m 273 km from as in the sloped bottom model domain described above.

For these experiments, forcing is chosen to minimize the effects of horizontal advection on the evolution of the temperature field. Furthermore, the choice of a modest

initial horizontal temperature gradient limits horizontal mixing so that primarily one-dimensional motions will be responsible for altering the temperature field. The initial temperature field for the experiments is achieved by cooling the surface of the model ocean over the sloping continental shelf topography. The ocean model is started from rest with constant salinity of 35 PSU and is initially linearly vertically stratified in temperature from 15° C at 200 m to 22° C at 70 m, and the upper 70 m is at a uniform temperature of 22° C. Inflow at the open boundary is relaxed to this temperature profile on a time scale of three days. A constant heat flux of -30 W/m^2 is applied to the surface for sixty days with an oscillating (sinusoidal) cross-shelf wind stress of 0.1 N/m^2 maximum amplitude and a period of six hours. Turbulent mixing due to convection and the surface momentum flux maintains a mixed layer of about 80 m. Thus, the water column is cooled uniformly with depth over the shelf, resulting in the shallow water being cooled faster than the deeper water as in *Pringle* [1998].

This resultant temperature field is applied to both the flat shelf and sloped shelf domains. The two models are restarted from rest and run for 20 days with an insulated surface and the surface momentum flux used during the cooling process. This allows both model oceans to adjust to equilibrium. The resulting cross-shelf temperature differences (from 28 km to 178 km offshore) for the two models after spin-up are 3.06° C for the sloped shelf and 3.01° C for the flat shelf. The models are then restarted using these states as the initial conditions for the heating experiment (Figure 6). The wind forcing used during the spin-up period is applied to both models, along with a 30 W/m^2 surface heat flux for sixty days.

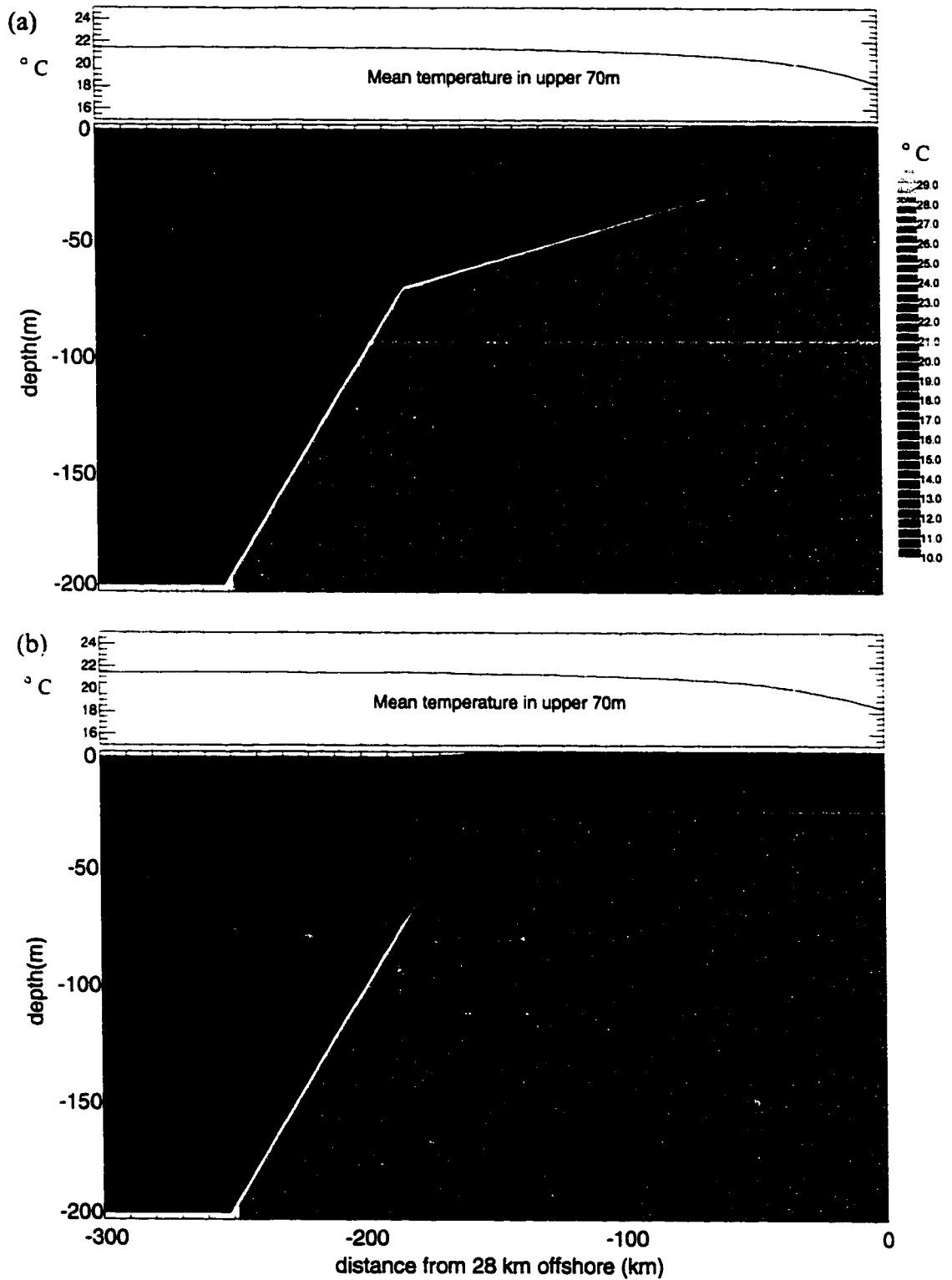


Figure 6. Initial conditions after spin-up for the sloped shelf (a) vs. flat shelf (b) experiment.

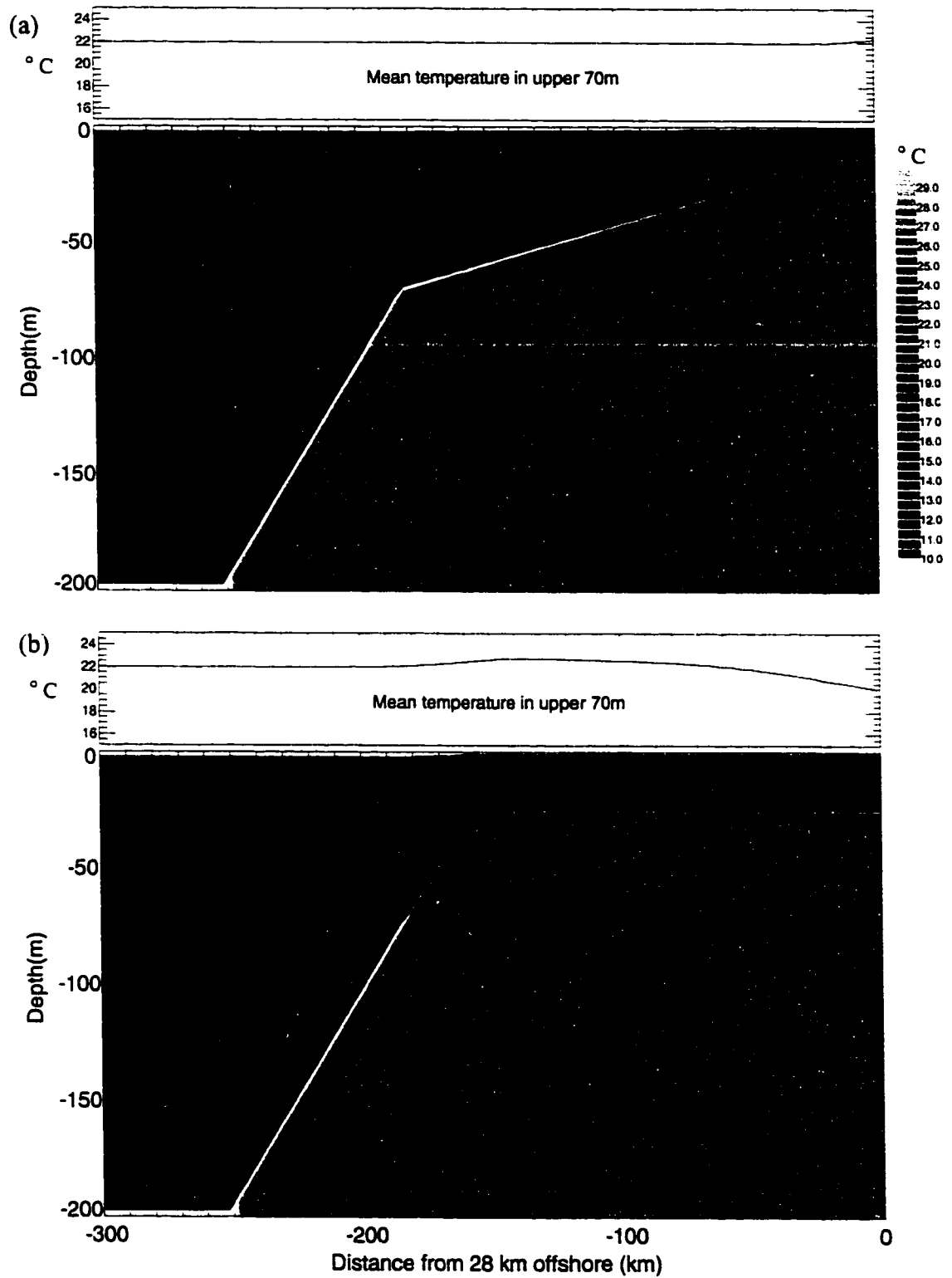


Figure 7. Temperature profiles and depth-averaged temperature for the sloped shelf (a) vs. flat shelf (b) experiment after 60 days of heating.

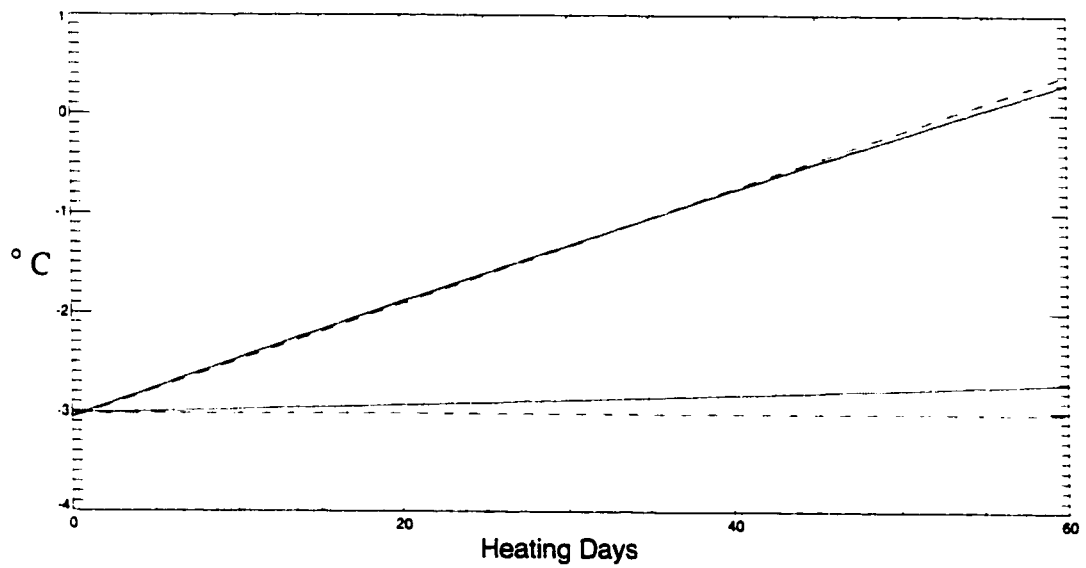


Figure 8. Difference in depth-averaged temperature over the continental shelf from 28 km offshore to 178 km offshore. The dashed lines are calculated using the time-integrated form of (24). The solid lines are calculated from the model temperature fields. Results for the sloped bottom are shown in black and the flat bottom results are shown in red.

Since ΔT for the water column is inversely proportional to the water column depth H in (24), the horizontal temperature gradient should remain over the flat continental shelf, but should weaken and reverse over the sloping shelf (Figure 7). The results from this experiment are in close agreement to the estimated ΔT calculated using the time-integrated form of (24) (Figure 8). As expected, the cross-shelf temperature difference from 28 km offshore to 178 km offshore for the flat shelf case is not reduced as it is in the sloped shelf case. Instead, the cross-shelf temperature difference is reduced by only 0.35°C over 150 km on the flat shelf. For the sloped shelf, the 3.01°C temperature difference is entirely eliminated and replaced with a 0.40°C difference in the opposite sense. The final cross-shelf temperature difference agrees to that calculated by (24) to within 0.09°C .

Naturally, these results must be viewed only as “thought experiments” as they are not really valid for the actual oceanic environment. Not only has highly idealized forcing been used, but also one would not expect the horizontal temperature gradient to ever form over a flat shelf (hence the necessity for running the sloped shelf model to generate the initial conditions). However, this experiment does serve to further illustrate the importance of the shelf slope to horizontal stratification. Additionally, it has been shown that (24) can suitably describe the heating rate of a water column in an ocean model using fully three-dimensional dynamics when horizontal motions are not dominant.

3.3 *The role of realistic forcing*

In the previous experiment, highly idealized (and rather unrealistic) forcing was applied to the model ocean to minimize horizontal motions so that the oceanic response

to the forcing was dominated by vertical mixing. The purpose was to determine if the heating of a water column could be adequately described by (24) if horizontal motions were allowed, but not dominant, and to determine how bottom slope plays a role in the horizontal stratification. It is necessary to study the response of the model ocean to forcing representative of realistic situations to determine if one can expect the relation (24) to be useful in describing the heating of a water column on a continental shelf in the real ocean.

For this experiment, the topography is chosen to represent the West Florida Shelf and the selected forcing is typical of that region. The West Florida Shelf is a wide continental shelf on which the spring transition in temperature stratification has been documented [*Florida Institute of Oceanography*, 1975] The model topography is identical to the sloping shelf domain described in the previous experiment results and is similar to the cross-shelf topography at 26° N on the West Florida Shelf (Figure 1). The domain is situated at 26° N with the shoreward direction aligned toward the east. The shelf region from the 10 m isobath to the shelf break will be the focus of the model results (Figure 9).

The ocean model is forced with spatially uniform daily NCEP Reanalysis [*Kalnay, et al.*, 1996] wind stresses and net surface heat fluxes from 1974 at 27.6° N, 84.4° W (Figure 10). These flux records are selected because they are typical of wintertime and springtime weather patterns in this area, and have clearly defined synoptic weather events that are useful for illustrative purposes. The wintertime weather pattern is dominated by the passages of synoptic-scale fronts with spatial scales of several thousand kilometers and time scales of several days. The most commonly observed fronts in this

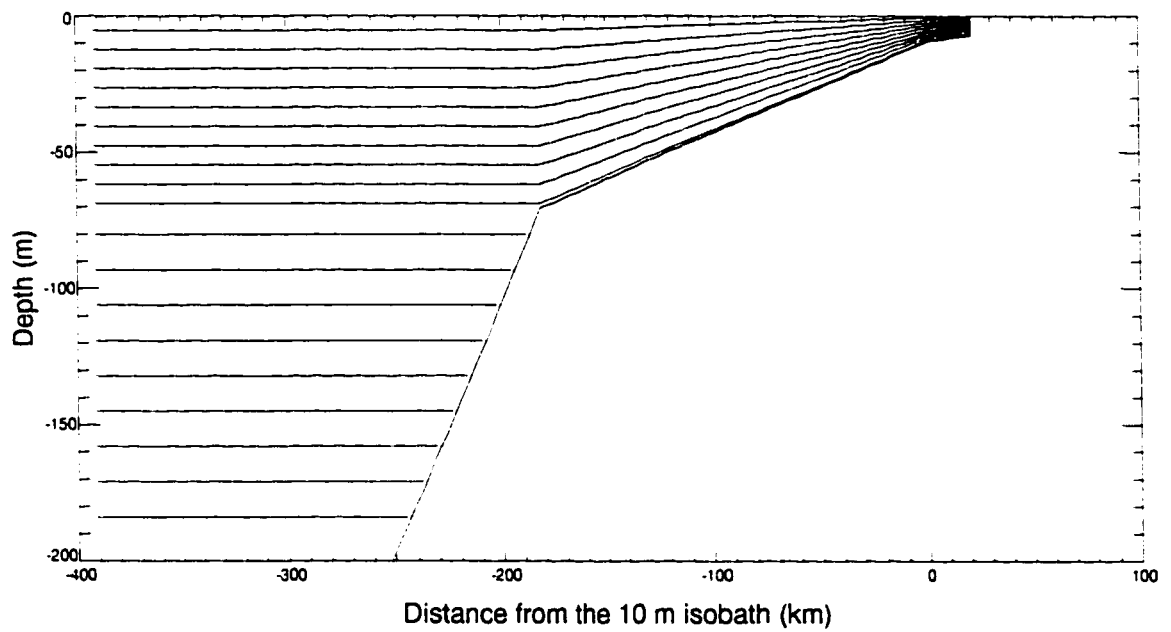


Figure 9. Vertical grid used in the SZM. 20 evenly spaced sigma coordinates are used above 70 m and 20 evenly spaced z-levels extend below 70 m to 200 m. The free surface is a sigma level. The horizontal grid spacing is 3.5 km. The center of every other vertical grid cell has been plotted.

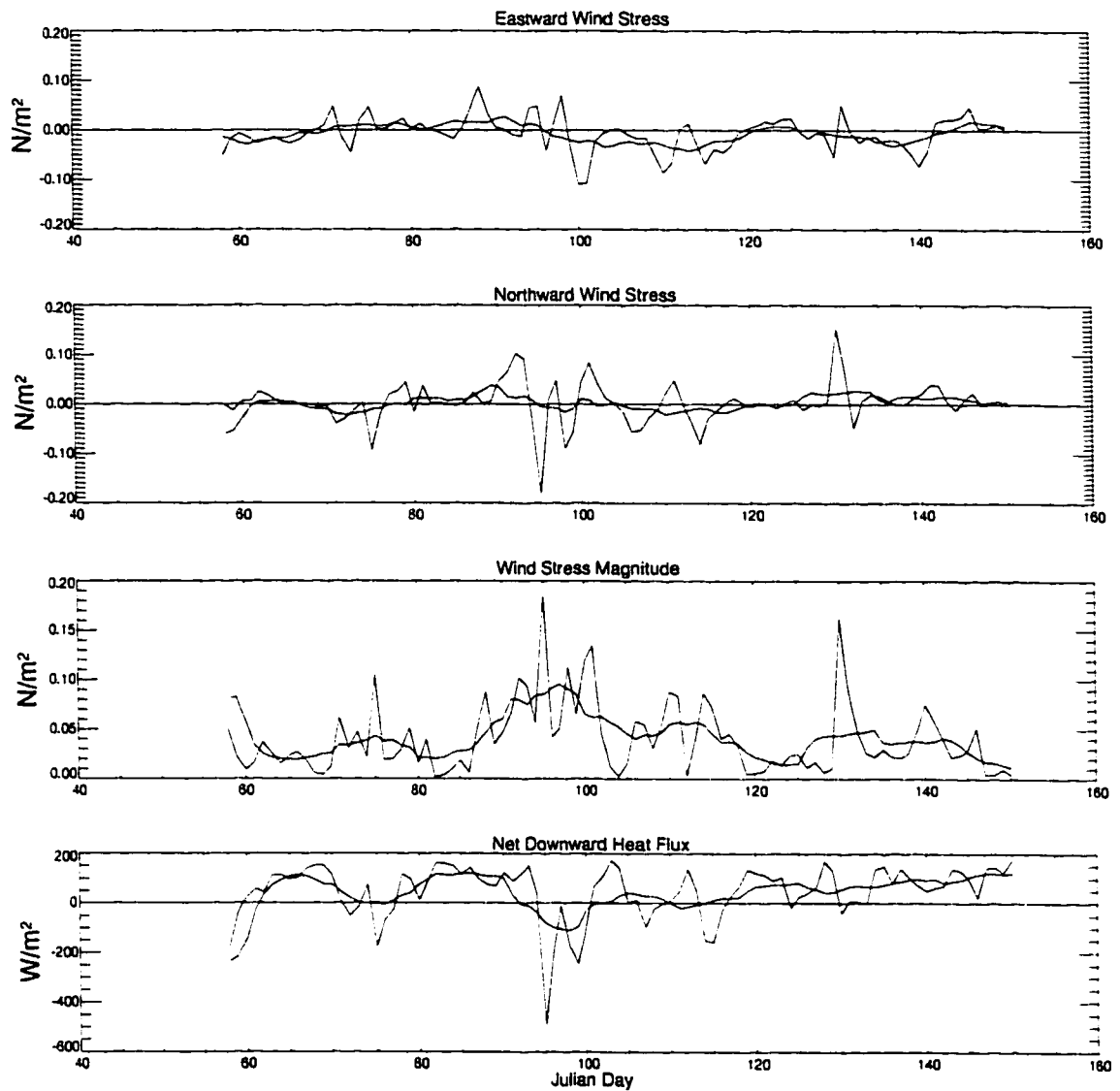


Figure 10. NCEP Reanalysis daily wind and net heat fluxes from 1974 at 27.6 N 84.4 W. A 9-day running average has been applied to the smooth overplotted line. The record has been plotted from Julian day 58 to 150, the duration of the model integration after the winter cooling.

region are cold fronts, which move toward the southeast and are characterized by a clockwise rotation of the local wind vector. Cold, dry air masses following the passages of cold fronts are associated with northerly winds with speeds typically 10 to 15 m/s and give rise to negative heat fluxes to the ocean's surface. These cold fronts become less frequent and produce less intense surface cooling of the ocean late in the season.

Springtime meteorological conditions are typified by periods of light winds and stabilizing heat fluxes followed by frontal passages with associated strong winds and often periods of surface cooling. A running average of the net surface heat flux shows a transition from surface cooling to a stabilizing heat flux in the early spring. Though the spring cold fronts are often associated with a negative heat flux, the heat flux averaged over several days remains positive for most of the season.

The ocean model is initialized in a state consistent with the wintertime stratification to best study the springtime transition. As in the earlier experiments, running the model with wind mixing and surface cooling produces this horizontally stratified state, however realistic fluxes from the NCEP data record are chosen in contrast to the idealized fluxes used in the earlier example. The ocean is initialized at rest with a homogeneous upper 70 m overlying the vertically stratified water as used previously. Surface momentum and heat fluxes from the 1974 data record are then applied from Julian day 1 to day 58. This allows sufficient time for the model to achieve a horizontally stratified state and to adjust to dynamic equilibrium. Julian day 58 follows the last frontal passage before the transition to a stabilizing heat flux. This transition is considered to be the beginning of the springtime weather pattern for this study and marks the beginning of

the transformation from the wintertime horizontal stratification to the summertime vertical stratification.

At Julian day 58, the transition marking the beginning of the warming heat fluxes, the ocean is mixed thoroughly to the bottom over the shelf with a cross-shelf temperature difference of 7°C (Figure 11a). During the next ten days, the light winds allow a thermocline to form between 5 m and 10 m under the stabilizing heat flux (Figure 11b). The heat input is confined only to the surface layer since the thermocline suppresses vertical mixing, thus preventing the vertical transport of heat to deeper water. The horizontal temperature gradient remains even in the presence of the thermocline. A weak cold front accompanied by a brief period of destabilizing heat flux reaching -180 W/m^2 and a maximum wind stress magnitude of 0.1 N/m^2 passes by day 76. The convective cooling and wind stirring weaken the thermocline and the surface mixed layer deepens to 10 m to 15 m over the shelf (Figure 11c). Where the depth of the surface mixed layer intersects with the bottom boundary layer, the water column is well mixed. The ocean is vertically mixed offshore to the 30 m isobath, and the vertical stratification over the deeper shelf is only about 1°C .

Though the cold front passing by Julian day 76 is accompanied by a negative heat flux, the time-integrated heat flux since the transition to the springtime warming period in day 58 remains positive. From day 58 to day 76, the time-averaged heat flux is 32.3 W/m^2 . This heat input to the surface of the ocean is distributed evenly with depth when the water column is mixed by the winds associated with the frontal passage. Since this heat input is spatially uniform, from (24) one expects the shallower water to have a larger increase in temperature. This effect is apparent by the reduction of the cross-shelf

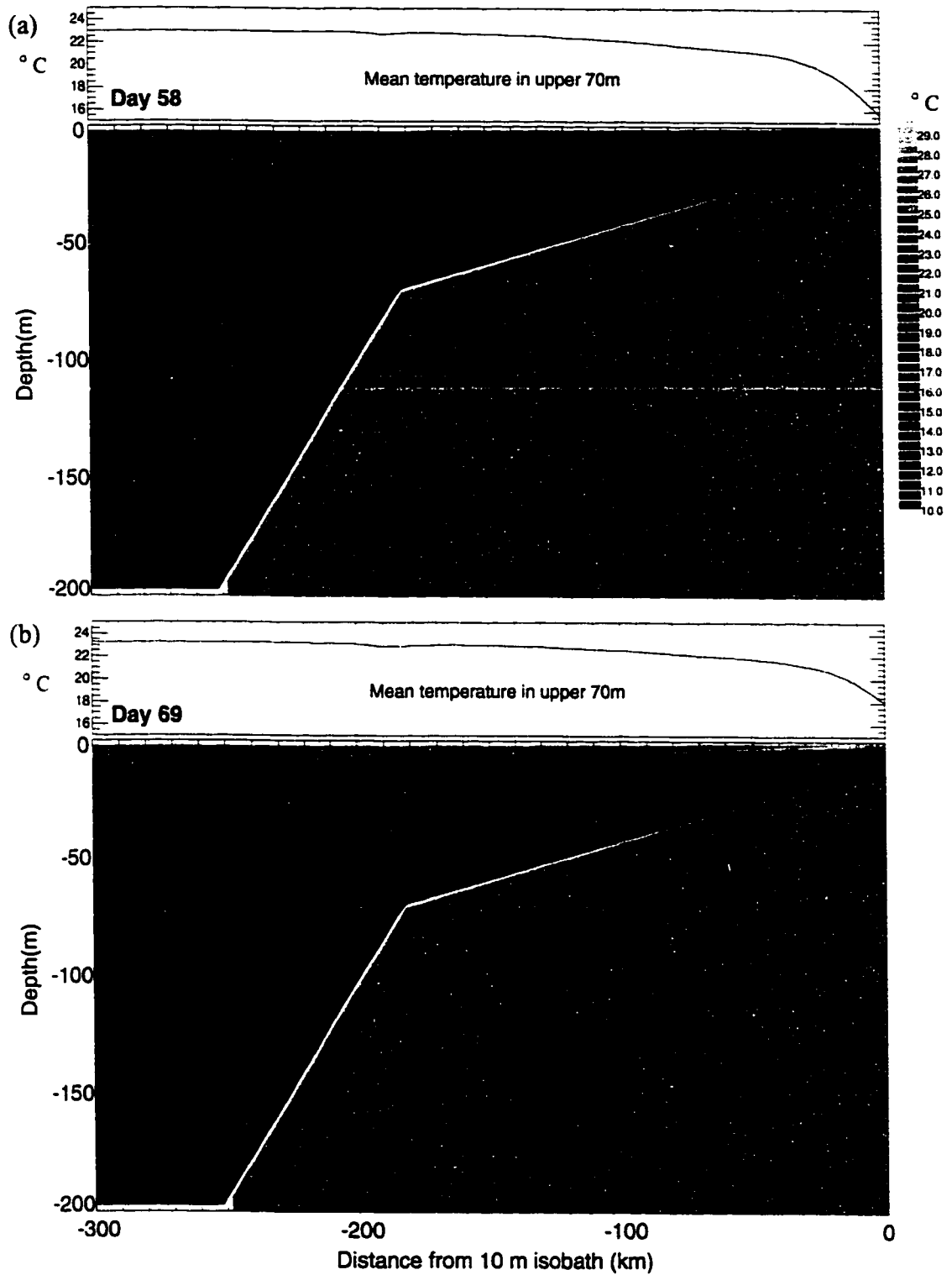


Figure 11. Temperature fields and upper 70 m depth-averaged temperatures from (a) Julian day 58, (b) day 69, (c) day 76, (d) day 116, (e) day 132, and (f) day 150. All model fields are spatially smoothed with a 1-2-1 smoother in the horizontal and vertical prior to plotting.

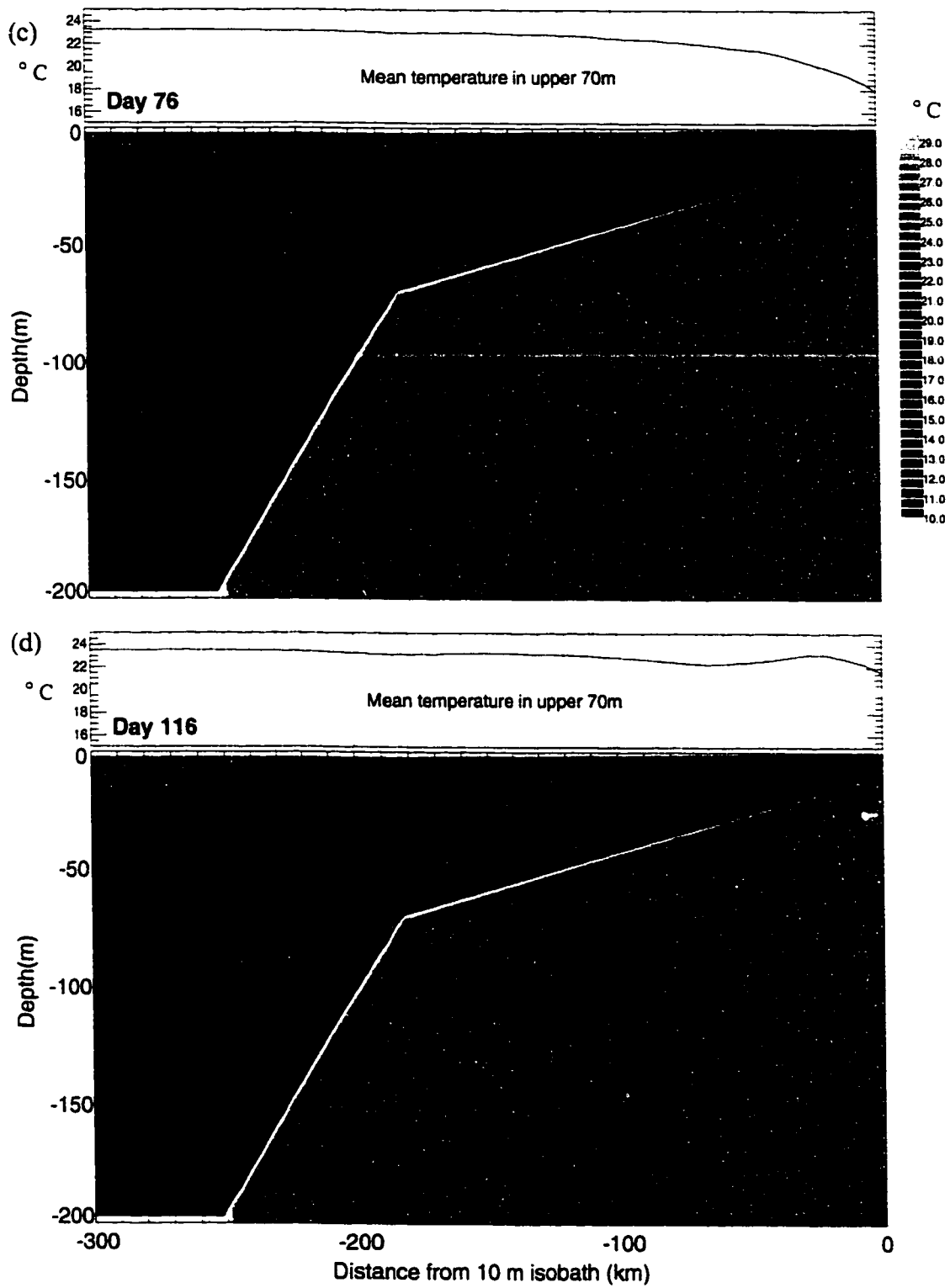


Figure 11. -continued

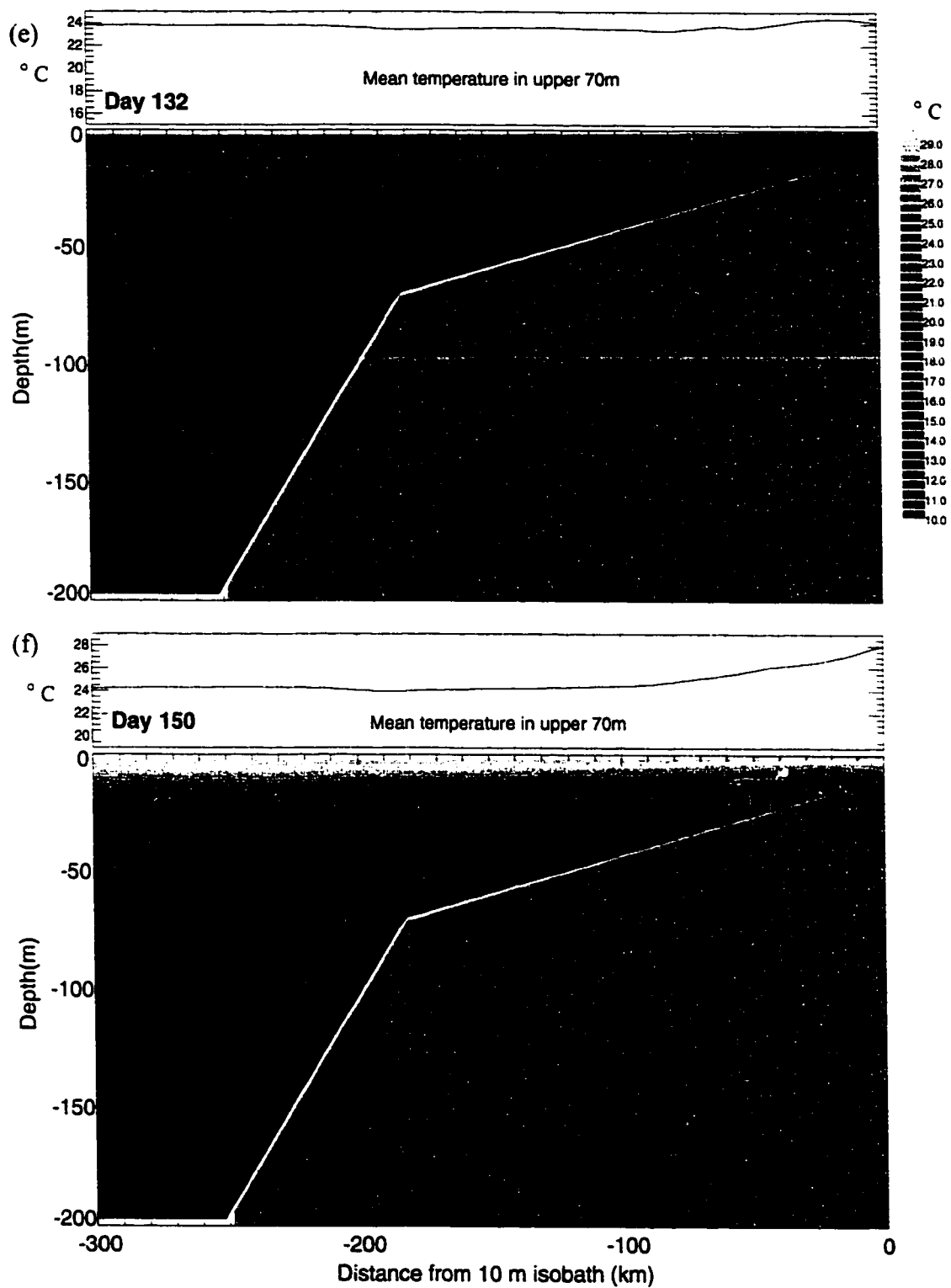


Figure 11. -continued

temperature difference from 7° C on day 58 to 5° C following the passage of the cold front on day 76. The mixing of the water column provides for warming at all depths so the horizontal temperature gradients are reduced equally at all depths over the inner shelf.

Following the frontal passage, the water column again stratifies under the stabilizing heat flux and light winds. This cycle of stabilization of the water column by surface heating and mixing of the water column resulting in uniform heating with depth continues throughout the spring. The squared buoyancy, or Brunt-Väisälä, frequency

$$N^2 = \frac{-g}{\rho_0} \frac{\partial \rho}{\partial z} \quad (27)$$

is a measure of the stratification of a water column (here, ρ is not a function of pressure).

$N^2=0$ indicates a mixed water column, while a stratified water column has a positive N^2 .

A time series of depth-averaged N^2 shows the cycle of stabilization and mixing of the water column in response to the surface fluxes of heat and momentum (Figure 12). The cycle is most apparent over the inner shelf where the mixing reaches the bottom. At each well-mixed state following a frontal passage, the horizontal temperature difference is weakened and eventually reversed (Figure 11c-e). The horizontal temperature gradient has been reduced to nearly zero by day 132. Additional heating and weak mixing later in the season reverse the temperature gradient such that it positive toward the coast. The thermocline is allowed to fully develop after the last frontal passage of the season (Figure 11f) completing the transition from the wintertime offshore temperature gradient to the summertime vertical temperature gradient.

It has been reported that the transition from the winter to summer regime is thought to be a rapid event that occurs soon after the last cold front of the season [*Florida*

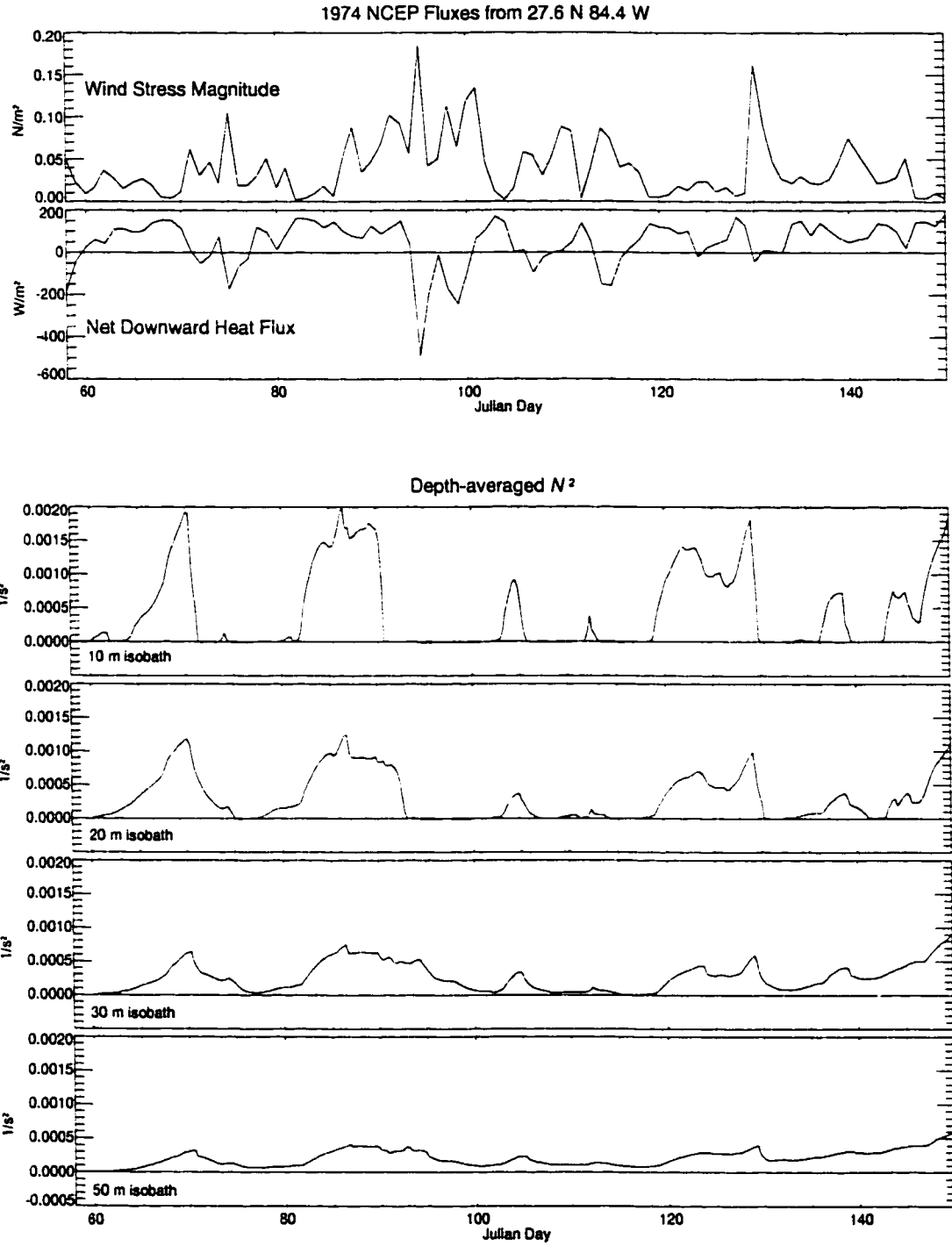


Figure 12. Depth-averaged buoyancy frequency squared (N^2) at the 10 m, 20 m, 30 m, and 50 m isobath on the continental shelf. The fluxes forcing the model are plotted for reference.

Institute of Oceanography, 1975], though the transition has never been precisely captured by observations. This present study concludes, however, that the transition is a two-step process. The relaxation and reversal of the horizontal temperature gradient (the first step) actually takes place throughout the spring with a time scale of about two months. The formations of the transient thermocline between fronts and following the last front (the second step) are, however, rapid events with a time scale of only a few days.

A description of the mechanism responsible for the formation of the transient thermocline is useful for achieving an understanding of the time scale for the water column stabilization. The gradient Richardson number

$$R_i = \frac{-\frac{g}{\rho_0} \frac{\partial \rho}{\partial z}}{\left(\frac{\partial u}{\partial z}\right)^2 + \left(\frac{\partial v}{\partial z}\right)^2} \quad (28)$$

represents the ratio of the density stratification and the vertical shear of the horizontal velocity (again, ρ is not a function of pressure). A negative R_i indicates an unstably stratified water column and turbulent mixing will intensify. A “small” R_i indicates that the shear production of turbulent kinetic energy dominates the stabilizing effects of buoyancy, and turbulent mixing is significant. A R_i that is considered “large” indicates that turbulent mixing is suppressed by the density stratification. The R_i above which mixing and turbulence ceases is known as the critical Richardson number. This has been estimated empirically to be $R_c = 0.23370$. Where R_i exceeds R_c , the turbulence is suppressed and the eddy diffusivity is reduced. When subject to a stabilizing buoyancy input, this will induce an even stronger stratification further suppressing turbulence. This

feedback mechanism leads to the formation of a thermocline across which both the turbulent kinetic energy flux and the buoyancy flux are diminished.

The role of the Richardson number is illustrated for the stabilization of the inner shelf water beginning on Julian day 116 following a frontal passage (Figure 13). On day 116, the inner shelf water is completely mixed vertically out to the 30 m isobath. Here, there is no depth where $R_i > R_c$ so turbulent motions maintain the homogeneity of the water column. A reduction in the wind stress and an increase in the heat flux over the next several days allow the water column to begin to stratify at mid-depth. R_c is exceeded so turbulent mixing of heat to the bottom is prevented. Thus, heating is confined only to the surface rapidly strengthening the vertical temperature gradient. The thermocline shallows as the wind stress magnitude reaches a minimum on day 119. A well-defined thermocline is apparent over the inner shelf on day 120.

A feature that is consistently apparent in the temperature fields throughout the record following Julian day 90 is a cold pool located at mid-shelf on the bottom. This cold pool has an effect on the depth-averaged temperature that is discrepant to what one would expect from (24). It is therefore necessary to elucidate the origin and persistence of this cold pool. The cold pool is formed during the week centered on Julian day 91 (Figure 14). The previous two weeks of stabilizing heat flux has stratified the shelf water so it behaves much like a two-layer system. A five-day period of southerly winds (Figure 10) causes downwelling resulting in offshore advection below the thermocline. This cold pool is advected far enough offshore that it has no contact with the surface during subsequent mixing events. It becomes essentially insulated due to the limited heat flux

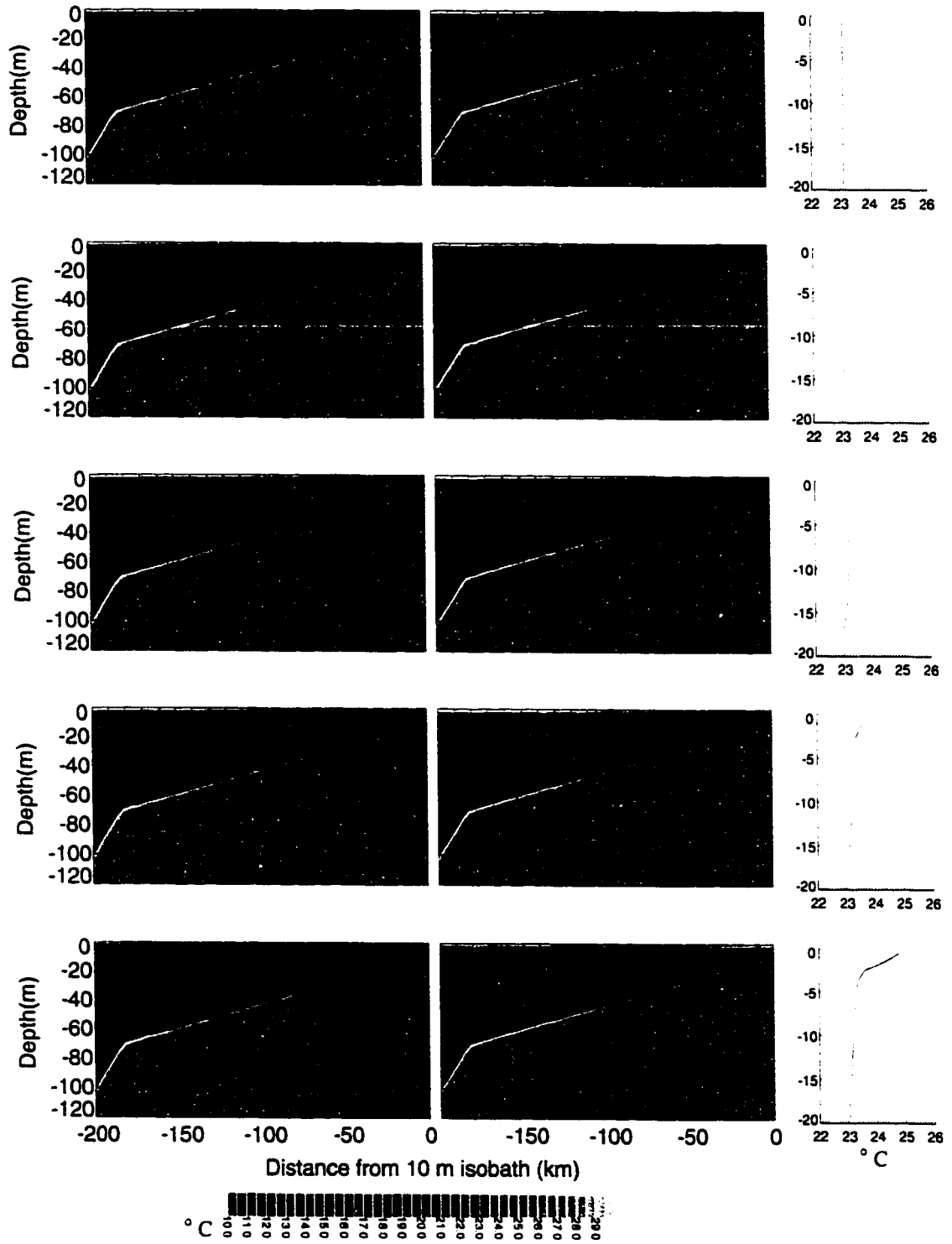


Figure 13. Critical Richardson number (R_c) contours (left), temperature fields (center), and temperature profiles from the 20 m isobath (right). Red areas indicate $R_i > R_c$ and blue areas indicate $R_i < R_c$.

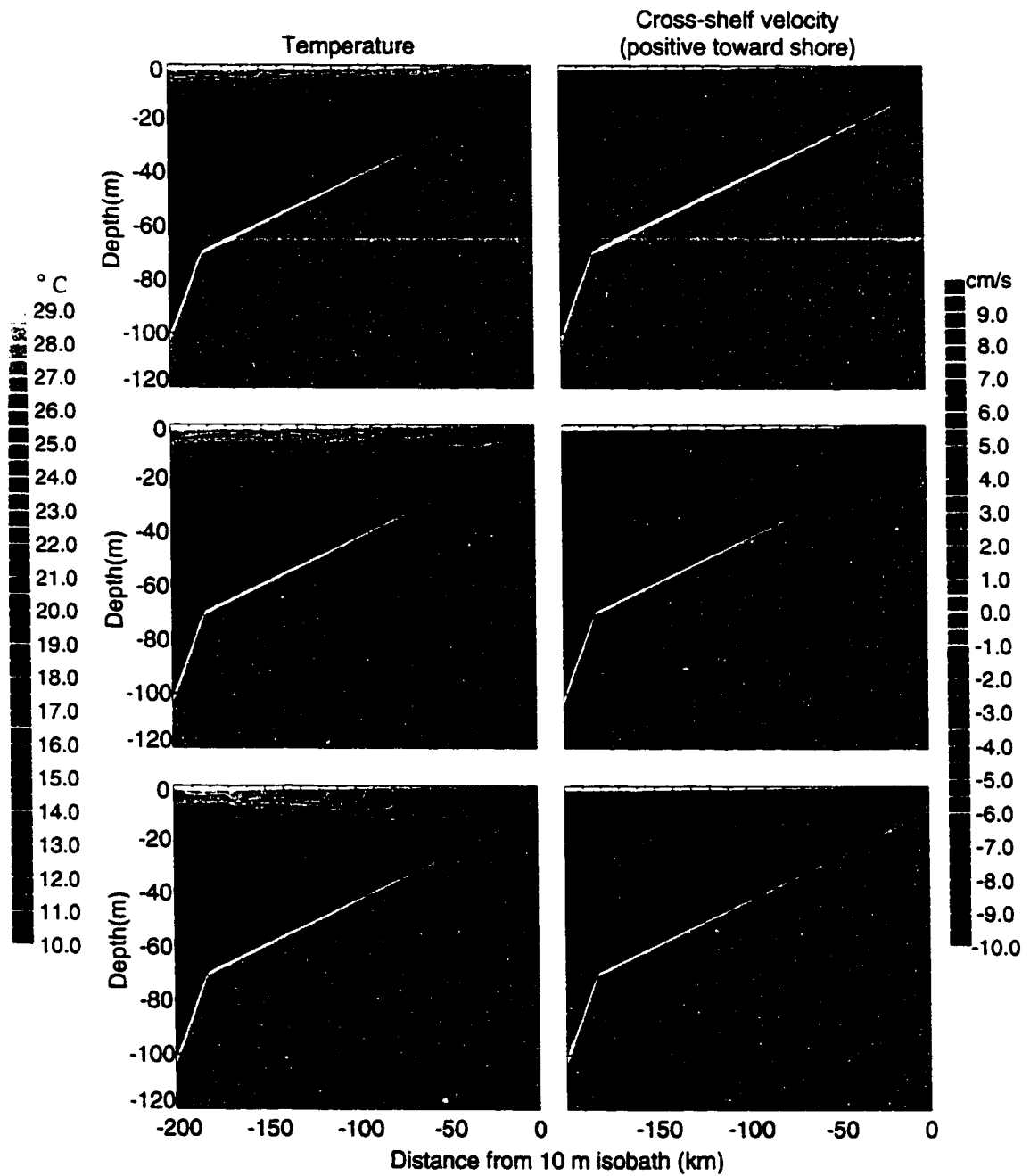


Figure 14. Temperature fields (left) and cross-shelf velocity (positive toward shore) (right) during the formation and offshore advection of the cold pool.

across the thermocline so it remains a persistent feature, and is still evident as a coherent structure on Julian day 150 (Figure 11f).

3.4 Analysis of the T -equation

It was earlier suggested that (24) might be useful in describing the change in horizontal stratification on a sloping continental shelf during the spring. When the assumptions associated with (24) are violated, as is the case when realistic forcing is used in a model where horizontal motions are allowed, it is no longer obvious that the simple model provides an adequate explanation to the problem. One must quantify the physical processes affecting the heating of the shelf water to determine the applicability of (24) to an ocean with realistic dynamics and forcing.

The change in depth-averaged temperature during a time interval t_0 to t_1 is found by depth-averaging the model temperature equation (8) subject to boundary conditions (13) and (17) and integrating in time yielding

$$\Delta \bar{T} = \frac{1}{\rho_0 c_p} \int_{t_0}^{t_1} \underbrace{\frac{Q}{h}}_A dt - \int_{t_0}^{t_1} \underbrace{\left(u \frac{\partial T}{\partial x} \right)}_B dt - \int_{t_0}^{t_1} \underbrace{\left(w \frac{\partial T}{\partial z} \right)}_C dt + \int_{t_0}^{t_1} \underbrace{\left(\frac{\partial}{\partial x} \left(A_H \frac{\partial T}{\partial x} \right) \right)}_D dt + \int_{t_0}^{t_1} \underbrace{\left(\frac{T(\zeta) - \bar{T}}{h} \frac{\partial h}{\partial t} \right)}_E dt \quad (29)$$

where

$$\overline{(\quad)} = \frac{1}{h} \int_{-H}^{\zeta} (\quad) dz \quad (30)$$

and $h = H + \zeta$. Equation (24) appears once again in a time-integrated fashion by equating the LHS of (29) with term A. A is the result of depth-averaging the vertical mixing term in the temperature equation and applying the surface and bottom boundary conditions. B

and **C** give the change in depth-averaged temperature due to horizontal and vertical advection of temperature. **D** is the change in the average temperature of a water column due to horizontal mixing. **E** owes its existence to variations in the free surface and has a negligible contribution to the temperature change of a water column, as will become evident.

Since equation (29) describes the change in depth-averaged temperature, it can be used to investigate the change in horizontal stratification at all depths when the limits of time integration correspond to well-mixed states. A term-by-term analysis of (29) therefore quantifies the contribution of each physical process responsible for the change in horizontal stratification between periods of vertical mixing (Figure 15). Because the horizontal temperature gradient is reduced to nearly zero at day 132 (Figure 11e), the results are shown for limits of time integration corresponding to the well-mixed states at day 58 and day 132, a 74-day integration.

It is clear that **A**, the vertical mixing term, accounts for the majority of the temperature change. The horizontal and vertical advection terms **B** and **C** act in the same sense on the temperature change of the water column and are largely responsible for the remainder of the heating. The horizontal mixing term **D** has little effect ($O(0.5^\circ \text{C})$) on the temperature change. The residual temperature change from **E** is a maximum of 0.26°C , supporting *a posteriori* the decision to consider this term insignificant.

Good physical understanding of the process responsible for the reduction of the wintertime horizontal temperature stratification by heating and mixing of the water column can be gained by the simple model (24), even when the full range of dynamics are present in the flow on the shelf. The balance $\text{LHS} = \text{A}$ describes the change in the

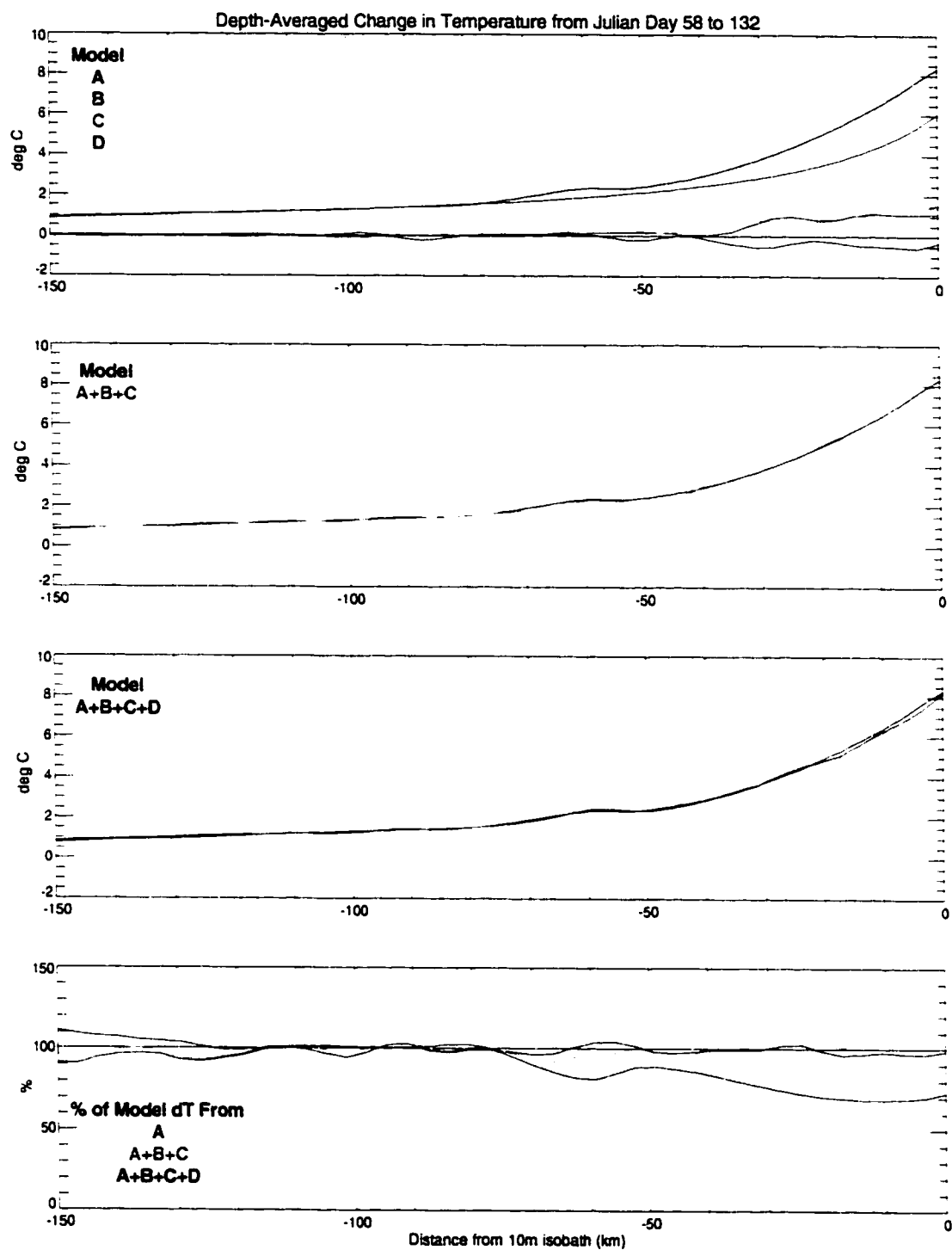


Figure 15. Term-by-term analysis of the depth-averaged temperature equation integrated in time from Julian day 58 to day 132.

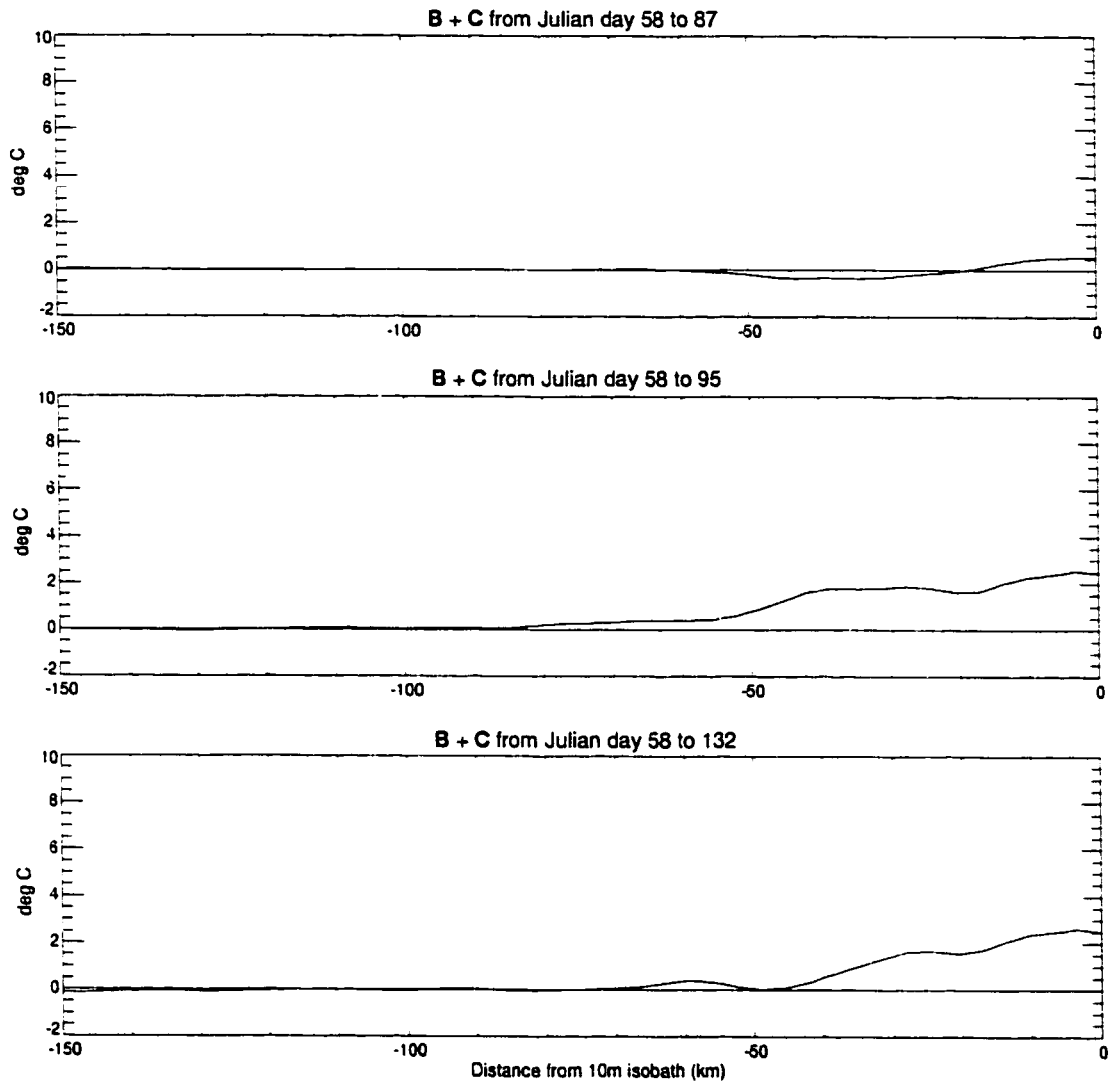


Figure 16. Change in depth-averaged temperature resulting from horizontal and vertical temperature advection since Julian day 58. The greatest temperature change over the integration period occurs during the cold pool formation and offshore advection.

depth-averaged horizontal stratification on the continental shelf to within a 31.0% error in this experiment. The average agreement on the shelf is to within 11.4%. The strongest deviations are in the shallowest water where the water column tends to heat faster than calculated by (24). This additional heating is due to horizontal and vertical temperature advection, and primarily occurs during downwelling events when the shelf water is stratified. Warm surface water flows toward shore and colder water below the thermocline is transported offshore resulting in accelerated warming of the inner shelf water. The effect of temperature advection on the temperature field for this experiment is most evident during the formation and offshore movement of the cold pool coincident with the week centered on Julian day 91 (Figures 14, 16).

4. DISCUSSION

The process by which the wintertime horizontal temperature gradient is eroded is not entirely unlike the process by which it forms. In the winter, a negative surface heat flux causes convective mixing enhancing the wind mixing. Over the shelf, the mixed layer reaches the bottom resulting in a homogeneous water column. The negative surface heat flux is distributed uniformly with depth bringing about a greater temperature reduction in shallower water than in a deeper water column. Thus, the nearshore water cools faster than the deeper shelf water resulting in the characteristic wintertime horizontal thermal gradient.

Previously, it was thought that the light winds and solar heating in the spring allowed the thermocline to form and it was not well understood how the horizontal temperature gradient was relaxed or reversed. The fallacy of this explanation lies in the fact that light winds and solar heating are equated with springtime weather over the temperate latitude continental shelves. It is the case, rather, that in a time-averaged sense, wind mixing of the water column and surface heating are not mutually exclusive over the course of the spring season. It is this realization that allows the application of (24) to the problem of the evolution of the temperature field throughout the spring.

The process responsible for the formation of the offshore thermal gradient in the winter reverses in the spring, except that convective mixing is limited only to brief

events. Strong winds associated with frontal passages are responsible for the periodic mixing of the water column. When appropriate conditions exist in the spring such that the ocean is being heated, but still vigorously mixed by wind forcing, this mechanism breaks down the horizontal offshore temperature gradient on a sloping shelf. These meteorological conditions are often found over mid-latitude continental shelves. Late winter and springtime frontal passages are followed by periods of positive downward heat flux and light winds. This allows the upper part of the water column to heat rapidly. As a new front passes, the water column is promptly mixed to the bottom over the inner shelf redistributing the heat from the surface evenly throughout the water column. The shallower inshore water is heated more rapidly than the deeper offshore water. After a series of these warming events and frontal passages, the offshore temperature gradient is relaxed or even reversed due to the faster heating of the shallower water. After the last strong wind event of the season, a thermocline can begin to form within a few days with a reduced or reversed offshore horizontal temperature gradient.

5. SUMMARY

The sloping bottom is responsible for the differential heating rates across the shelf. In a shallow body of water with constant depth subject to a spatially uniform heat flux, only horizontal mixing and advection can play a role in determining the horizontal stratification. The heating rate described by (24) is inversely proportional to the water column depth so that a shallower water column will heat more rapidly than a deeper water column subject to the same positive heat flux. Continental shelf dynamics have been simulated using the SZM forced by daily heat and momentum fluxes at the surface to determine the applicability of the simple analytical model to realistic oceanic conditions. The computation and comparison of each term of the depth-integrated time-averaged temperature equation quantifies the significance of the physical processes that can alter the temperature field. The simple model used to describe the heating rate of a water column subject to one-dimensional mixing appears as the dominant balance in the integrated temperature equation. Calculation of the depth-averaged temperature change from the surface heat flux using (24) agrees to the SZM model results of the realistic simulation to within 31% over the shelf. The spatially averaged error is only 11.4%. Horizontal and vertical advection during periods of downwelling result in faster heating over the inner shelf than predicted by the simple model.

The spring transition of the thermal stratification over a wide sloping shelf in a temperate location has now been fully described by two processes. The first is the erosion of the horizontal thermal gradient as calculated by (24), and modified by temperature advection and only weakly by horizontal mixing. This occurs on a time scale of about two to three months, dependent upon the local weather, when the water column is being heated and mixed periodically. The second process is the formation of the seasonal thermocline following the last strong mixing event of the spring season. This occurs on a time scale of less than a week under a stabilizing heat flux and light winds completing the spring transition from horizontal to vertical thermal stratification.

REFERENCES

- Artale, V., A. Provenzale, and R. Santoleri, A process of thermocline erosion on the Sicilian continental shelf, *Il Nuovo Cimento*, 11, 1988.
- Asselin, R., Frequency filter for time integrations, *Mon. Wea. Rev.*, 100, 487-490, 1972.
- Beardsley, R. C., D. C. Chapman, K. H. Brink, S. R. Ramp, and R. Schlitz, The Nantucket Shoals Flux Experiment (NSFE79) Part 1: A basic description of the current and temperature variability. *J. Phys. Oceanogr.*, 15, 713-748, 1985.
- Bigelow, H. B., Studies of the waters on the continental shelf, Cape Cod to Chesapeake Bay 1: The cycle of temperature, *Papers Phys. Oceanogr. Meteor.*, 2, 1933.
- Bigelow, H. B. and M. Sears, Studies of the waters on the continental shelf, Cape Cod to Chesapeake Bay. 2: Salinity, *Papers Phys. Oceanogr. Meteor.*, 4, 1935.
- Burrage, D. M., and R. W. Garvine, Summertime hydrography at the shelf break front in the Middle Atlantic Bight, *J. Phys. Oceanogr.*, 18, 1309-1319, 1988.
- Caruthers, J. W., *Fundamentals of Marine Acoustics*, 153 pp., Elsevier, New York, 1977.
- Chapman, D. C. and G. Gawarkiewicz, On the establishment of the seasonal pycnocline in the Middle Atlantic Bight, *J. Phys. Oceanogr.*, 23, 2487-2492, 1993.
- Clarke, A. J., Overview of the physical oceanography of the Florida shelf in the study region, Proceedings from the Northeastern Gulf of Mexico Physical Oceanography Workshop, Clarke, A. J. ed., Florida State University, Tallahassee, FL, 1994.
- Clarke, A. J., and K. H. Brink, The response of stratified, frictional flow of shelf and slope waters to fluctuating large-scale, low-frequency wind forcing, *J. Phys. Oceanogr.*, 15, 439-453, 1985.

- Florida Institute of Oceanography, Compilation and summation of historical and existing physical oceanographic data from the eastern Gulf of Mexico, Report to Bureau of Land Management, Contract #08550-CT4-16, St. Petersburg, FL, 97pp., 1975.
- Gilbert, W. E., A. Huyer, E. D. Barton, and R. L. Smith, Physical oceanographic observations off the Oregon coast, 1975: WISP and UP-75, *Oregon State University Data Report 64*, 189 pp., Oregon State University, Corvallis, Oregon, 1976.
- Haney, R. L., On the pressure gradient force over steep topography in sigma coordinate ocean models. *J. Phys. Oceanogr.*, *21*, 610-619, 1991.
- Houghton, R. W., F. Aikman III, and H. W. Ou, Shelf-slope frontal structure and cross-shelf exchange at the New England shelf-break, *Contin. Shelf Res.*, *8*, 687-710, 1988.
- Kalnay, E., M. Kanamitsu, R. Kistler, W. Collins, D. Deaven, L. Gandin, M. Iredell, S. Saha, G. White, J. Woollen, Y. Zhu, M. Chelliah, W. Ebisuzaki, W. Higgins, J. Janowiak, K. C. Mo, C. Ropelewski, J. Wang, A. Leetmaa, R. Reynolds, R. Jenne, and D. Joseph, The NCEP/NCAR 40-year reanalysis project, *Bull. Amer. Meteor. Soc.*, *7*, 437-471, 1996.
- Mann, K. H., and J. R. N. Lazier, *Dynamics of Marine Ecosystems*, 466 pp., Blackwell Scientific Publications, Boston, 1991.
- Martin, P. J., An ocean model with a combined sigma and z-level vertical coordinate system, Naval Research Laboratory, Stennis Space Center, MS, (in prep.) 1998.
- Martin, P. J., G. Peggion, and K. J. Yip, A comparison of several coastal ocean models., Technical Report NRL/FR/7322—97-9672, Naval Research Laboratory, Stennis Space Center, MS, 1998.
- Mellor, G. L., and T. Yamada, Development of a turbulence closure model for geophysical fluid problems, *Rev. Geophys. And Space Phys.*, *20*, 851-875, 1982.
- Millot, C., The Gulf of Lions' hydrodynamics, *Contin. Shelf Res.*, *10*, 885-894, 1990.
- Niiler, P. P., Observation of low-frequency currents on the West Florida continental shelf, *Mem. Soc. Roy. Sci. Liege*, *10*, 331-358, 1976.
- Pringle, J. M., Cooling and internal waves on the continental shelf, Dissertation, 225 pp., Massachusetts Institute of Technology, Cambridge, Massachusetts, 1998.
- Noh, Y. and H. J. S. Fernando, Onset of stratification in a mixed layer subjected to a stabilizing buoyancy flux, *J. Fluid Mech.*, *304*, 27-46, 1995.

Orlanski, I., A simple boundary condition for unbounded hyperbolic flows, *J. Comput. Phys.*, *21*, 251-269, 1976.

Stech, J. L., and J. A. Lorenzetti, The response of the South Brazil Bight to the passage of wintertime cold fronts, *J. Geophys. Res.*, *97*, 9507-9520, 1992.

Symonds, G. and R. Gardiner-Garden, Coastal density currents forced by cooling events, *Contin. Shelf Res.*, *14*, 143-158, 1994.

BIOGRAPHICAL SKETCH

Degrees

B.S. Mathematics, 1995, University of Missouri – Columbia
B.S. Computer Science, 1995, University of Missouri – Columbia
M.S. Oceanography, 1997, Florida State University
Ph.D. Oceanography, 1999, Florida State University

Publications

Morey, S. L., Shriver, J. F., and J. J. O'Brien, The effects of Halmahera on the Indonesian Throughflow, *J. Geophys. Res.*, In press, 1999.

Murray, C. P., Morey, S. L., and J. J. O'Brien, Interannual variability of upper ocean vorticity balances in the Gulf of Alaska, *J. Geophys. Res.*, Submitted, 1999.

Honors

National Defense Science and Engineering Graduate Fellowship, 1995-1998
University Fellowship, FSU, 1998-1999
Outstanding Graduate Student Award, 1999

Professional Organizations

American Geophysical Union

Field Experience

R.V. *Seminole*, March, 1996
NOAA Ship *Ka'imimoana*, August – September, 1996